ChemInform Abstract: DC Voltammetry of Electro-Deoxidation of Solid Oxides

ARTICLE *in* CHEMINFORM · JUNE 2013

Impact Factor: 0.74 · DOI: 10.1002/chin.201325189

4 AUTHORS, INCLUDING:

A. Cox

University of Cambridge

23 PUBLICATIONS **222** CITATIONS

SEE PROFILE

Derek Fray

University of Cambridge

316 PUBLICATIONS **5,756** CITATIONS

SEE PROFILE

CHEMICAL REVIEWS

Review

pubs.acs.org/CR

DC Voltammetry of Electro-deoxidation of Solid Oxides

A.M. Abdelkader,*[,†] K. Tripuraneni Kilby,[‡] A. Cox,[‡] and D. J. Fray[‡]

[†]School of Materials, University of Manchester, Grosvenor Street, Manchester, U.K., M1 7HS

[‡]Department of Materials Science and Metallurgy, University of Cambridge, Pembroke Street, Cambridge, U.K., CB2 3QZ

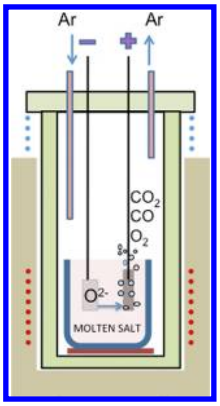

CONTENTS

1. INTRODUCTION

Using electric current as a tool in metallurgy dates back to the early years of the nineteenth century. Davy and Berzelius discovered alkali metals were able to be electrolyzed from their molten salts when large number of Volta cells were connected in series in the early nineteenth century.[1] However, it was only in 1869 that the first industrial electrolytic cell was introduced near Swansea for the electrorefining of copper.[2] Heroult and Hall achieved another significant advance in 1886 when, simultaneously but independently, they patented a new process for producing aluminum by the electrolysis of a fused bath of cryolite (Na_3AlF_6) containing Al_2O_3. Over years, considerable developments in the production and purification of metals and alloys via electrometallurgical techniques have been achieved.[2]

Electrorefining is a frequently used electrometallurgical technique. Traditionally, electrorefining involves the purification of metals by anodically dissolving the impure metal, followed by plating-out of pure metals on the cathode. However, Ward and Hoar refined molten copper by making it a cathode in molten $BaCl_2$. A constant current was applied and nonmetallic impurities were ionised and discharged on the carbon anode, leaving pure copper on the cathode.[3] A few decades later, Okabe and his co-workers used the same principle to cathodically remove atomic oxygen from titanium and other reactive metals.[4] It was claimed that under a constant voltage of 3 V applied between the titanium cathode and carbon anode in molten $CaCl_2$, the deoxidizer, calcium, is produced on the cathode according to reaction 1. Calcium is then able to deoxidize the titanium according to reaction 2, with the oxygen ion removed from the system as CO or CO_2 gas by reactions 3 and 4:[4]

$$Ca^{2+}(\text{in } CaCl_2) + 2e^- = Ca(\text{on Ti cathode}) \quad (1)$$

$$O(\text{in Ti}) + Ca = Ca^{2+}(\text{in } CaCl_2) + O^{2-}(\text{in } CaCl_2) \quad (2)$$

$$O^{2-}(\text{in } CaCl_2) + C(\text{anode}) = CO(g) + 2e^- \quad (3)$$

$$2O^{2-}(\text{in } CaCl_2) + C(\text{anode}) = CO_2(g) + 4e^- \quad (4)$$

At the end of the twentieth century, Chen et al.[5] investigated the electrochemical removal of alpha case on titanium and its alloys. Again the material to be deoxygenated was made the cathode and carbon used as an anode in molten $CaCl_2$. A

Received: August 4, 2011
Published: January 22, 2013

   dx.doi.org/10.1021/cr200305x | Chem. Rev. 2013, 113, 2863–2886

constant voltage between 2.8 to 3.1 V was applied to avoid chlorine evolution.[5] Partial deoxygenation was observed in a sample electrolyzed at 2.5 V, and hence it was concluded that the process could proceed by oxygen ionization without the need for depositing calcium at unit activity from CaO that was dissolved in the melt.[5] This finding led to the emergence of a new technology, named after its inventors (Fray−Farthing−Chen) as the FFC-Cambridge process, for producing reactive metals by the reduction of their oxides in molten salt.

The FFC Cambridge Process can be summarized by taking titanium oxide as an example: TiO_2 powder is used as a cathode in the form of pellets or presintered rectangular coupons incorporating a conducting wire. This cathode is then immersed in a molten salt electrolyte (conventionally $CaCl_2$) with a graphite anode. Electrolysis occurs at a cathodic potential below the potential for the deposition of calcium at unit activity, in order to ionize the oxygen from the cathode, to allow it to dissolve into the electrolyte, and then to remove it as O_2, CO, or CO_2 at the anode. The following reactions can be considered:[5b,6]

at the cathode

$$TiO_2 + 4e - = Ti + 2O^{2-} \tag{5}$$

at the anode

$$2O^{2-} = O_2(g) + 4e^- \tag{6}$$

Later on, it was proven that the FFC Process can also be applied to many other metal oxides, for example, Cr_2O_3, Nb_2O_5, ZrO_2, Ta_2O_5, SiO_2, WO_3, and CeO_2. The additional benefit of using the FFC Process is that the mixture of metal oxides can also be reduced directly to alloys and intermetallic compounds, for example, TiNi, $TiAl_3$, Ni_3Al, TiNb, Ti-6Al-4 V, and Ni_2MnGa.[7]

These laboratory observations, together with further pilot tests carried out at Cambridge, and also with research conducted by other independent institutions, started the commercialization of this process. In 1998, a new company British Titanium plc was formed to explore the FFC invention for titanium-based metals. A further step was taken when FFC Ltd. was spun-out of Cambridge University in early 2002 to use the FFC-Cambridge process for the exploitation of all metals, except titanium. In April 2003, the company changed its name to Metalysis, Ltd.

The FFC-Cambridge process, like any other electrochemical process, has four variables; current, potential, time, and concentration of the electroactive species. In recent years, many different DC voltammetric techniques have been used in order to understand the reduction mechanisms, or to optimize the process parameters. These techniques include constant voltage, constant potential, cyclic voltammetry, and constant current. This article will review the research, thus far undertaken, to understand the behavior of different oxides during the course of the electrode-oxidation process.

2. THEORETICAL CONSIDERATIONS

There are two different interpretations for the reduction mechanisms. The first mechanism, named the OS (Ono−Suzuki) process, is an electrochemical reaction in which the electron transfer step involves the deposition of metallic calcium from CaO in the electrolyte and the chemical reaction step that results in the calciothermic reduction of the metal oxide (reactions 7 and 8).[8] The second mechanism is the FFC-Cambridge process, involving only an electron-transfer-type reaction in which the metal oxide is directly reduced to metal requiring no calcium generation (reaction 9), with the oxygen ions becoming free to leave the cathode, to diffuse in the electrolyte, and to discharge at the anode.

$$nCa^{2+} + 2ne^- = nCa \tag{7}$$

$$nCa + MO_x = MO_{x-n} + nCaO \tag{8}$$

$$MO_x + 2xe^- = M + xO^{2-} \tag{9}$$

In fact, the combined reactions 7 and 8 of the OS mechanism leads to the same end result as eq 9. However, there is a large body of evidence that distinguishes between the two mechanisms: (1) the direct electrochemical reduction of most of the known metal oxides, with the exception of some rare earths oxides, is thermodynamically possible at a lower cathodic potential than that is required to form Ca from CaO. Even after forming a metal−oxygen solid solution with oxygen content at the parts per million level, the oxygen ionization is still more thermodynamically favorable than the reduction of CaO. (2) The reductant in the OS mechanism, either by Ca^+ or metallic calcium, is generated in a separate step allowing the reduction of the metal oxide to take place in any location in the cell and not necessarily on the cathode; while the direct electrochemical reduction takes place only at the cathode. In fact, Suzuki et.al. proposed an experimental arrangement in which the electron transfer step and the chemical reduction steps were conducted in separate vessels.[8c]

There are some disadvantages relating to the deposition of calcium: (1) the generated calcium metal increases the electronic conductivity of the molten salt and consequently increases the nonfaradic current and parasitic reactions raising the energy consumption. (2) Under the conditions of decomposing CaO, the direct electrochemical reduction will also participate in the reduction. However, the rate of oxygen removal could be slower as a layer of calcium metal on the surface would hinder the diffusion of the oxygen ions.

To determine the thermodynamic feasibility of a half-cell reaction, such as that presented by eq 9, it is worthwhile to start by considering the Nernst equation for that reaction:

$$E = E^\circ - \frac{RT}{nF} \ln \frac{a_M \cdot a_{O^{2-}}^x}{a_{MOx}} \tag{10}$$

At unit activity ($a = 1$), the logarithmic term is equal to zero and the standard electrode potential, E°, can be calculated from eq 11

$$E^\circ = -\frac{\Delta G^\circ}{nF} \tag{11}$$

Equation 11 is used to calculate the minimum potential required to ionize oxygen from various metal oxides in the literature.[7b,9] Table 1 shows the standard electrode potentials E° corresponding to the direct electro-deoxidation of a number of metal oxides. The calculations were performed from the known thermodynamic data at 1173 K using HSC Chemistry 6.1,[10] with a Ca^{2+}/Ca reaction assigned a standard reduction potential of zero.

However, the electro-deoxidation process is far more complicated than that represented in single-step linear equations linking free energy with logarithmic functions of composition. The interaction between the oxide cathode and the electrolyte, the different electroactive species existing in the

dx.doi.org/10.1021/cr200305x | Chem. Rev. 2013, 113, 2863−2886

Table 1. Selected Standard Reduction Potentials for the Cathode in Fused Chlorides at 1173 K, Assuming All Species Are in Standard State, at Unit Activity

reaction	E° (V)
$O_2 + 4e^- = 2O^{2-}$	2.657
$NiO + 2e^- = Ni + O^{2-}$	1.970
$CoO + 2e^- = Co + O^{2-}$	1.880
$2FeO + 4e^- = 2O^{2-} + 2Fe$	1.800
$WO_3 + 6e^- = W + 3O^{2-}$	1.720
$MoO_2 + 4e^- = Mo + 2O^{2-}$	1.682
$2K_2O + 4e^- = 2O^{2-} + 4K$	1.593
$2/5Nb_2O_5 + 4e^- = 2O^{2-} + Nb$	1.376
$2/3Cr_2O_3 + 4e- = 2O^{2-} + 4/3Cr$	1.323
$SiO_2 + 4e^- = 2O^{2-} + Si$	0.843
$TiO_2 + 4e^- = 2O^{2-} + Ti$	0.761
$2/3Al_2O_3 + 4e^- = 2O^{2-} + 4/3Al$	0.407
$ZrO_2 + 4e^- = Zr + 2O^{2-}$	0.370
$HfO_2 + 4e^- = Hf + 2O^{2-}$	0.272
$2MgO + 4e^- = 2O^{2-} + 2Mg$	0.208
$2Ca^{2+} + 4e^- = 2Ca$	0.000

molten bath (such as alkali metal cations, CO_3^{2-}, dissolved complexes from the cathode, etc) and the composition changes occurring on the cathode or in the electrolyte, are all factors which complicate the thermodynamic calculations of the electro-deoxidation process, as each possible reaction needs to be similar to eq 10. Summarizing the thermodynamic data involved in each oxide-metal−electrolyte system is particularly useful in understanding the behavior of oxide in contact with molten electrolyte under particular set of conditions. Littlewood diagrams map out the possible stable phases in molten salts by resembling the treatment of Pourbaix diagrams for corrosion in aqueous solutions, with the modification that the basicity of the system is written in terms of pO^{2-}, where $pO^{2-} = -\log a_{O^{2-}}$.[11] B. Tremillon and later on G.S. Picard from the "Ecole Nationale Superieure de Chimie de Paris" have conduct extensive work to assemble similar E/pO^{2-} stability diagrams for the oxides in molten salts particularly for systems involved in nuclear industry.[12] Recently, Inman et al,[13] used the same approach to construct the E/pO^{2-} diagram for the system Ca−Ti−O−Cl to understand the behavior of titanium oxide during the electro-deoxidation in molten calcium chloride. The predominance diagram of the systems Ca−Ti−Ni−O−Cl, Ca−Mo−O−C, and Ca−W−O−Cl have also been constructed by the same group[14]

For a molten calcium chloride salt, calcium and chlorine are generated at potentials below and above the reduction and oxidation potentials limits of the molten bath. To maintain consistency, the formation of unit activity calcium (eq 12), at 1173 K, is chosen as the reference point.[13] This is assigned a standard Gibbs free energy change of zero, which consequently sets its standard electrode potential as zero ($E^\circ_{Ca} = 0$ V). The formation of chlorine (eq 13) at unit atmosphere partial pressure (E°_{Cl2}) is therefore 3.214 V. However, it is also necessary to know the electrode potentials for calcium and chlorine formation at other activities and partial pressures respectively. These can be calculated through the corresponding Nernst equations (eqs 14 and 15).[13] It should be noted that the natural logarithm has been replaced by the logarithm to the base of ten.

$$Ca^{2+} + 2e^- = Ca \tag{12}$$

$$Cl_2 + 2e^- = 2Cl^- \tag{13}$$

$$E_{Ca} = E^\circ_{Ca} - \frac{2.303RT}{nF} \log a_{Ca} \tag{14}$$

$$E_{Cl} = E^\circ_{Cl} + \frac{2.303RT}{nF} \log P_{Cl_2} \tag{15}$$

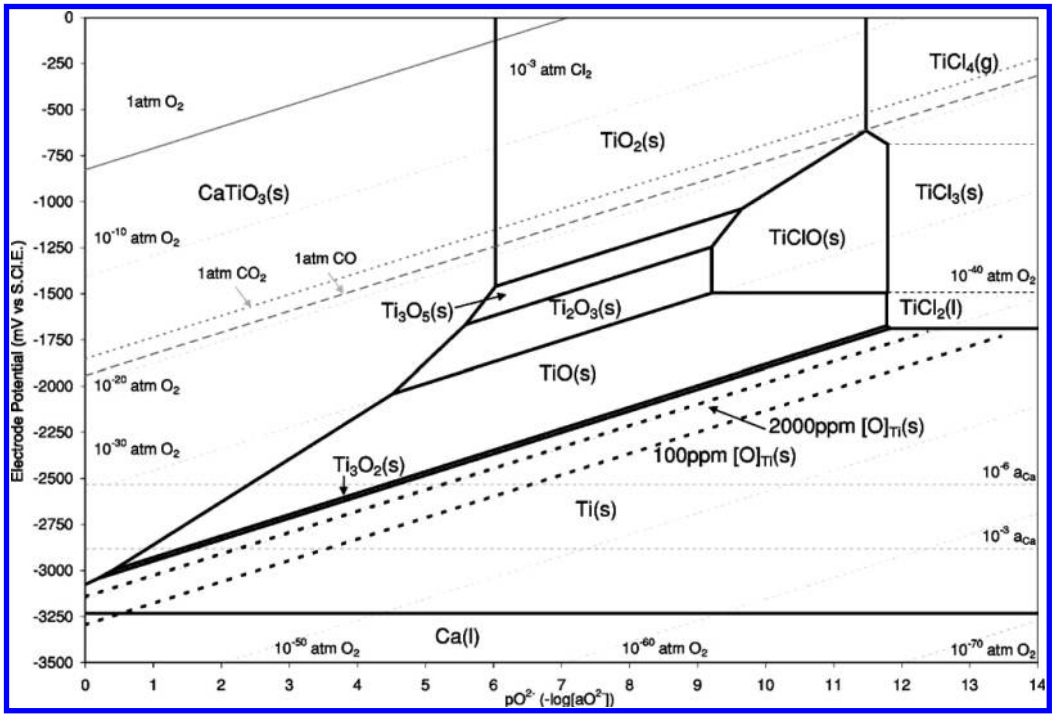

Figure 1. E/pO^{2-} diagram for the Ti−Ca−O−Cl system at 1173 K with CO and CO_2 evolution on a graphite anode.[13] Reprinted with permission from ref 13. Copyright 2005 the Electrochemical Society.

dx.doi.org/10.1021/cr200305x | Chem. Rev. 2013, 113, 2863−2886

The oxygen and oxide ions can be introduced to the system after defining the standard state of the oxide ion by choosing dissolved CaO, at unit activity.[13] The partial pressure of oxygen gas and the activity of oxide ions in the melt, expressed in terms of its negative logarithm, may be calculated from its respective half-cell reactions (reaction 16) at any given potential according to the corresponding Nernst equation (eq 17)

$$\frac{1}{2}O_2 + 2e^- = O^{2-} \tag{16}$$

$$E_{O^{2-}} = E^{\circ}_{O^{2-}} + \frac{2.303RT}{2nF}\log(P_{O_2}^{(1/2)}/P_{O^{2-}}) \tag{17}$$

Similarly, incorporation of other species (including titanium and its associated oxides, chloride, and oxychloride compounds) to the E/pO^{2-} diagram is possible, through the same convention and known thermodynamic data.[13] The standard states were assigned to be unit activity for the condensed phases and unit partial pressure for the gas phases. The resulting E/pO^{2-} diagram has titanium of higher oxidation states on the top part, with the lower states more stable at a lower potential. Equation 17 gives rise to a straight-line dependence of E on pO^{2-} at a given oxygen pressure. Therefore, for reactions independent of pO^{2-}, such as reduction of $TiCl_4$ to $TiCl_3$ and $TiCl_3$ to $TiCl_2$, a horizontal line will represent the potential at which the two species can coexist in molten $CaCl_2$. In contrast, for reactions that are not involved in electron transfer processes, such as the chlorination of TiO_2 to $TiCl_4$, a vertical line represents the oxygen partial pressure at which the two compounds are in equilibrium. The regions within the boundaries define a phase field of unit activity. For example, the domain marked as $TiCl_4$, the only compound of titanium which might exist at unit activity (unit partial pressure in this case) is $TiCl_4$, but any other species, such as Ti^{4+}, Cl^-, and O^{2-}, might also exist in the melt.

The usefulness of the E/pO^{2-} diagrams in context of the FFC-Cambridge process might be made clearer by introducing the equilibrium of oxygen dissolved in titanium in Ca−O−Cl systems at the temperatures of interest. Using the free energy change calculated by Okabe et al,[15] three equilibria lines of oxygen content in titanium metal at a given potential and melt oxide activity were superimposed in the E/pO^{2-} diagrams. It is immediately noticeable from the predominance diagrams for the Ca−Ti−O−Cl (figure 1) that the production of low-oxygen titanium may occur at significantly different potentials, depending on the pO^{2-} of the melt. However, at low pO^{2-}, potentials near the standard state electrolyte decomposition are required which might result in the undesired deposition of calcium. On the other hand, at high pO^{2-} the calcium titanate phases are very stable and are reduced at higher cathodic potentials.

3. ELECTRO-DEOXIDATION UNDER CONTROLLED VOLTAGE OR POTENTIAL

The potential calculated in Table 1 or presented in the predominance diagrams is simply the theoretical minimum potential that must be applied to the cathode for the oxygen to be removed. Achieving the required potential at one electrode and maintaining it constant (or varied according to certain programmes) throughout an experiment is possible by using a potentiostat, which forces current through the working electrode to maintain a defined potential difference between the latter and a reference electrode. However, applying a constant voltage between the anode and the cathode in a two-terminal cell is more favored industrially because of its simplicity in construction and operation. Most research carried out to investigate the viability of the electro-deoxidation process was conducted under a controlled cell voltage (mostly constant) or controlled potential conditions of the cathode.

The current−time curves obtained when operating the FFC-Cambridge at either constant cathode voltage or constant cell voltage showed a similar trend, that is, the current decays with time. The dependence of current on time for a single electrode can be described by the Cottrell equation (eq 18). Deviations from eq 18 occur as a result of convection effects[16] or because of coupled chemical reactions. However, that is not always the case as the mass transfer in the electro-deoxidation process not only takes place through the surface diffusion layer, but also inside the electrode materials, which might complicate the current−time representation

$$i = \frac{nFCAD^{1/2}}{\pi^{1/2}t^{1/2}} \tag{18}$$

where i is current in A, n is number of moles, F is Faraday's constant in $C\cdot mol^{-1}$, C is concentration of the electroactive species in $mol\cdot cm^{-3}$, A is electrode surface area in cm^2, D is the diffusion coefficient in $cm^2\cdot s^{-1}$, and t is time in seconds.

3.1. Earlier Attempts to Describe the Reduction Mechanism

The classical controlled voltage in a two-electrode system was the first electrochemical technique used by FFC-Cambridge process researchers.[17] The voltage across the cathode−anode pair was adjusted to maintain the potential difference below that required to decompose the salt but high enough to break the anion−cation bond in the oxide cathode. Under such conditions, the current is flowing at a rate proportional to rate the electrochemical reactions to satisfy the cell voltage. Recording the behavior of the current over the electrolysis time was used to deduce the electrode reactions of which the current is a response.

In the early published papers, it was suggested that the shape of the current−time curves depends on the conductivity of the oxide and the solubility of oxygen in the metal.[9a,18] In case of titanium, the current rises to a peak and then declines gradually to a very low value, while for chromium, on the other hand, the current profile shows a peak which gradually declines to a plateau value before it reduced to the background current.[9a] Therefore, it was concluded at this early stage of the process investigations that the rate-limiting step in metals that have high oxygen solubility is the diffusion of oxygen in the metal. On the other hand, in case of chromium, or other metals with low oxygen solubility, the rate determining step is diffusion of oxygen ions held in the pores of the reduced pellet.[18]

It was then found, by taking niobium as an example, that the initial value and the behavior of the current depends on the porosity and, perhaps, on the effective surface area of the pellets.[19] For denser pellets, the initial current was markedly lower than that of porous pellets, and the overall rate of electro-deoxidation was substantially lower. The change in the current rate during the electro-deoxidation of Nb_2O_5 was thought to be due to the formation of various niobium oxides with lower oxidation states.[19] This was the first time the use of partially reduced samples was reported to determine the reduction pathway. The XRD analysis of the samples electrolyzed for 0.5, 1, 2, and 4 h indicated the presence of various calcium niobate

dx.doi.org/10.1021/cr200305x | Chem. Rev. 2013, 113, 2863−2886

phases associated with the niobium lower oxides.[19] Moreover, formation of the niobate phases was attributed to the increase of CaO activity within and around the porous pellets because of O^{2-} ions.[19] Subsequently, this was shown to be incorrect as there is always some CaO in the melt.[20]

Upon plotting ln I against time, Yan et al[21] observed a liner relationship after 5 h of electro-deoxidation . It had been concluded from the linearity, and by expressing the limiting current using eq 19, that the rate of the electro-deoxidation was likely controlled by the diffusion of the oxygen ions in the niobates toward the niobate/melt interface.[21] However, the linearity of the relationship over the last 40 h of electro-deoxidation, that is, after the niobate phase vanishes, has not been rationalized.

$$I_1(t) = I_0(t)\ \exp^{(-D_oA/V\delta_o t)} \tag{19}$$

where $I_1(t)$ and $I_1(0)$ are the current at time t and the initial current in the limiting current region, respectively, A is the surface area of the niobates exposed to the melt, D_o is the diffusivity of the oxygen ions in the niobate, δ_o is the thickness of the diffusion layer, and V is the volume of the niobate.

3.2. Three-Phase Interline (3PI) Propagation Models

Since the initial investigations of the FFC-Cambridge process, a change in color was observed in the parts of the pellet in direct contact with the current collector after few minutes of applying the current.[18] It was believed that the reaction starts from these areas and progress toward the pellet core.[22] To test this assumption, Chen et al[23] scrutinized the changes arising through the cross section of a porous chromium oxide pellet electrodeoxidized for 30 min. The SEM and EDX analysis indicated the existence of two phases: a "high-purity chromium" phase on the surface and an oxide phase at the core of the pellet. On the basis of these findings, the authors proposed that the electro-deoxidation of metal oxides starts at the metal/oxide/electrolyte three phase interlines (3PIs).[23]

The 3PIs can be understood as follows:[24] (1) the reduction of the metal oxide begins at the 3PIs that exist next to the current collector, (2) the metallized part of the pellet then operates as a current collector, and (3) the 3PIs move to the boundary of the reduced part. The propagation of the reduction process is then determined by the movement of the 3PIs either transversally by "The thin layer 3PIs (T3PIs) model" or longitudinally by "The penetrating 3PIs (P3PIs) model". Metallization in the surface layer is much faster than that within the pellet core.

The model was verified during the electro-deoxidation of quartz in molten $CaCl_2$ at 1123 K. The potentiostatic experiments used a 20 mm-diameter quartz pellet as a working electrode, two graphite rods as a counter electrode, and a quartz sealed Ag/AgCl reference electrode.[24a] The behavior of the current−time curve during the course of the electro-deoxidation was straightforwardly explained through the 3PIs: (1) the initial increase in current was explained by the expansion of the 3PIs on the surface thin layer, and (2) the reduction subsequently progresses into the bulk of the oxide and hence the current declines. Also, and in agreement with the P3PI model, the reduction of the quartz pellet in the depth direction was observed to proceed with the formation of uniform thickness layers of silicon. The L^2-t curve (L is the thickness of the reduced layer at time t) exhibits a linear relation, which is expected from the mathematical representation of the P3PI model. The product IL (where I is the current density), shows invariable behavior after long electrolysis which again confirms the mathematical representation of the P3PI model. The experimental findings also reveal that the current increased as the applied potential became more negative.

The current−time curve recording during the electro-deoxidation of titanium dioxide and chromium sesquioxide has also been explained through the 3PIs concept in a way similar to the silica case. The current increases in the first stage because of the increase of the 3PIs length, and reaches its peak when the surface layer is completely metallized.[25] Subsequently, the current then decreases because of the slow rate propagation of 3PIs in the depth direction. The morphology of the generated metallic particles during their growing stage was also connected to the 3PIs concept. As the 3PI propagates into the interior of the pellet, oxygen ions are removed from the oxide surface, and the formed metallic atoms tend to form clusters rather than a continuous layer creating physical gaps between the oxide and the metal.[25] Therefore, newly formed metal atoms have to diffuse through the interface and join the less energetic cluster. These clusters tend to form a spherical or a nodular nucleus, which keeps their shape during its growth, forming metal particles up to few micrometers in size. If the formed particles have the chance to grow more, more regular shaped crystals will be formed since the preferential growth of crystal is at the low-density planes.[25]

3.3. Alkali Ternary Oxides Intermediates

In general, insertion of electrons into a solid oxide cathode can lead to either the ionization of the oxygen in the oxide, and the dissolution of these ions into the electrolyte, or the reduction of metal cations from the electrolyte to achieve electrical neutrality. According to the removal of oxygen, the electro-deoxidation reaction is expected to take place in several steps through different oxidation states because of the multivalent nature of most metal oxides. On the other hand, intercalation between the electrolyte and the oxide cathode forms binary oxide phases having the formula $A_xM_yO_z$ where A is the alkaline earth metal cation from the molten bath; M is the metal ion to be reduced; and x, y, and z are integers. However, the overlapping involved between oxygen ionization and cation incorporation is anticipated by considering the thermodynamic and kinetics of the reactions. Examining partially reduced samples, either under constant voltage, or under controlled cathodic potential, was used to investigate the changes occurring in the pellet during the course of electro-deoxidation and consequently to deduce the electro-deoxidation pathway and understanding the microstructural kinetics of the process.

3.3.1. Niobium Oxide. Niobium oxide was the first metal oxide that was subjected to a consistent study in which the electro-deoxidation was terminated after different times in order to examine the partially reduced samples. Under a constant voltage of 3.1 V, Yan et al[19] observed calcium niobates phases after 24 min of electro-deoxidation . Although these niobate phases were associated with various lower oxidation states of niobium oxides, they increased the overall oxygen content from 20.54 to 22.25 wt % between electro-deoxidation time of 70 and 126 min.[19] After 250 min, the oxygen content was reduced by 92.78 wt % and the sample was almost metallic niobium with some traces of the niobate phases.[26] The latter was reported to disappear after prolonged electro-deoxidation .[19,26a] It has also been reported that the slowest step of the electro-deoxidation is the removal of oxygen from the Nb−O solid solution at the later stage of the process.[26a] Xu et al

dx.doi.org/10.1021/cr200305x | Chem. Rev. 2013, 113, 2863−2886

claimed that the formation of the calcium niobate prior to the electro-deoxidation increases the overall process rate.[27]

3.3.2. Tantalum Oxide. Tantalum's chemical properties are broadly similar to that of niobium, and one could expect the electro-deoxidation of Ta_2O_5 to be similar to that of Nb_2O_5 by passing through different intermediate phases of oxidation states decreasing in the order $Ta^{5+} \rightarrow Ta^{4+} \rightarrow Ta^{3+} \rightarrow Ta^{2+} \rightarrow$ Ta. However, Barnett[28] reported that all the intermediate calcium tantalum oxides were in the +5 oxidation state. The proposed pathway was summarized in the following scheme:[28]

$$Ta_2O_5 \rightarrow CaTa_4O_{11} \rightarrow CaTa_2O_6 \rightarrow Ca_2Ta_2O_7 \rightarrow Ca_3(CaTa_2)O_9 \rightarrow Ta$$

A similar pathway was observed in a eutectic $CaCl_2$–NaCl and $CaCl_2$–NaCl –CaO melt.[29] Song et al[29] reported that the reduction follows a series of calcium tantalum oxides in the form $(Ta_2O_5)(CaO)n$ with n = (0, 0.5, 1, 2, 4). The values of n increase by increasing the concentration of CaO in the melt. Again, none of these intermediate phases can be considered reduced. However, upon fixing the potential of the cathode at −0.7 V versus Ag/AgCl reference electrode in molten $CaCl_2$, it was possible to detect TaO and δ-TaO phases.[30] The reduction mechanisms were accordingly modified by Wu et al.[30] to include another intermediate step in which TaO reduces to Ta metal.

Microstructurally, the transformation of one phase to another is always associated with destroying and reconstructing the grains into the distinct crystal structure of the emerged phase. This series of destroying–reconstructing steps remove the coherent network initially present in the Ta_2O_5 pellet.[28] Moreover, the produced Ta does not sinter at the applied temperature. Therefore, the final product in the form of nodules in submicrometer size that are interconnected into larger aggregates (2–5 μm).[28,30] The oxygen content of the nodular Ta was 6700 ppm after applying constant voltage of 2.7 V for 8 h in molten $CaCl_2$–CaO.[28] The three-terminal cell mode produces much lower oxygen content (1200 ppm) after only 5 h of electro-deoxidation at a constant potential of −1.2 V versus a Ag/AgCl reference electrode.[30]

3.3.3. Chromium Oxide. Although niobium was the first example in which a partially reduced sample was analyzed to investigate the reduction mechanisms, chromium was the first to link the phase changes with the current–time curve as a response of the electrochemical reactions taking place.[23] The sample taken directly after the initial peak in the time–current curve showed metallic chromium at the surface layer of the pellet, and chromium oxide at the core, which according to the oxygen analysis, had undergone partial reduction. A transition layer containing calcium chromite, $CaCr_2O_4$, was observed between the two zones. After 2 h of electro-deoxidation at 2.8 V constant voltage, the internal sections of the pellets were dominated by the chromites indicating how quickly the chromite formed.[23] The rate of reducing the chromite phases was found to be dependent on the pellet and electrolysis parameters but in general only a minor chromite content was observed in the sample taken after the first current–time plateau, suggesting that the reduction was almost finished.[31] These results were confirmed by the low oxygen content of the obtained powder.[31]

For greater control of the cathodic processes, Schwandt[20] et al. used three-terminal cell by incorporating graphite pseudo reference electrode. The potential of a chromium sesquioxide cathode was increased at a rate of −0.3 V/hour, which was then maintained at −1.0 V versus the graphite pseudoreference electrode. The current increased to a peak at the target potential and then reduced gradually to the background value. The sample taken at the peak was a mixture of Cr_2O_3, $CaCr_2O_4$, and Cr. By allowing more charge to pass through the cathode, the amount of Cr metal increased and that of Cr_2O_3 decreased.[20] It was concluded from this result that "chromium occurs in the oxidation states three and zero only" and the metallisation of Cr_2O_3 passes through the formation of the calcium chromite $CaCr_2O_4$.[20] It was proven experimentally that $CaCr_2O_4$ was produced electrochemically by inserting calcium ions from the electrolyte through eq 20, and then reduced to chromium through eq 21, with oxygen being discharged at the anode.[20] Another key point from this work is as follows:

> *Calcium exists exclusively in the oxidation state two throughout the entire electro-deoxidation process. Although calcium ions play an active role in the reduction process and are temporarily found in the cathode, they are never discharged, and calcium metal is never formed. Therefore, the reduction proceeds in an entirely electrochemical manner and no calciothermic reaction step is required.*[20]

$$4Cr_2O_3 + 3Ca^{2+} + 6e^- = 2Cr + 3CaCr_2O_4 \quad E^\circ_{1173K} = 1.560\ V \tag{20}$$

$$CaCr_2O_4 + 6e^- = 2Cr + 3Ca^{2+} + 4O^{2-} \quad E^\circ_{1173K} = 0.778\ V \tag{21}$$

3.3.4. Titanium Oxide. Titanium dioxide is the traditional example used to study the electro-deoxidation process. The reduction mechanisms and kinetics under constant voltage and controlled potential conditions have been subjected to a large number of investigations in many laboratories across the globe.[6b,32] Wang et al.[32a] suggested a two step reduction($TiO_2 \rightarrow TiO \rightarrow Ti$) based on step voltage tests. They also concluded from measuring the AC impedance spectra of a TiO_2 bar that the charge transfer resistance and activation energy of the two reactions increases as the cathode overvoltage increases.[32a] Schwandt et al.[32r] have studied the TiO_2 electro-deoxidation pathway under constant voltage. The voltage was initially kept at 2.5 V and then increased to 2.9 V in a three-stages regime.[32r] By analyzing partially reduced samples at different times, it was concluded that the electro-deoxidation of TiO_2 is taking place in four stages. In the first one, titanium dioxide reacts with Ca^{2+} to produce lower oxides and perovskite calcium titanate.[32r]Th-These suboxides are then reduced to TiO by the action of Ca^{2+}, with more perovskite produced as a byproduct. Chemical reactions then occur between TiO and $CaTiO_3$, and a lower-valent calcium titanate $CaTi_2O_4$ is produced.[32r] In the final stage, $CaTi_2O_4$ is electrochemically reduced to TiO, which is then further reduced to Ti through the formation of Ti–O solid solution, $Ti[O]_\delta$.[32r]The reaction sequence is presented by eqs 22–26, and the standard electrode potential for each reaction is compared versus a Ca^{2+}/Ca reference point, at 1173 K.[32r]

$$5TiO_2 + Ca^{2+} + 2e^- = Ti_4O_7 + CaTiO_3 \quad E^\circ \approx 1.807\ V \tag{22}$$

dx.doi.org/10.1021/cr200305x | Chem. Rev. 2013, 113, 2863–2886

$$4Ti_4O_7 + Ca^{2+} + 2e^- = 5Ti_3O_5 + CaTiO_3 \quad E^\circ = 1.678\ V \tag{23}$$

$$3Ti_3O_5 + Ca^{2+} + 2e^- = 4Ti_2O_3 + CaTiO_3 \quad E^\circ = 1.575\ V \tag{24}$$

$$2Ti_2O_3 + Ca^{2+} + 2e^- = 3TiO + CaTiO_3 \quad E^\circ = 1.200\ V \tag{25}$$

$$TiO + 2(1-\delta)e^- = Ti[O]_\delta + (1-\delta)O^{2-} \quad E^\circ \approx 0.177\ V \tag{26}$$

It was then claimed, "the ex-situ perovskitization can significantly increase the speed and efficiency of the electro-reduction of solid TiO_2 in molten $CaCl_2$".[32f] Therefore, some attempts to dope titanium oxide with calcium oxide prior to electrolysis were conducted,[32k] and the hypothesis was then enlarged to include the electro-deoxidation of other oxides.[27,32v,33] However, microstructure kinetic investigations showed that the overall reduction rate is not only determined by the rate of the individual electrochemical reaction, or diffusion, but also with the method of forming the intermediate perovskite compounds.[32s] Formation of the face-centered cubic NaCl crystal structure of the TiO from the less dense higher oxides, which usually have a rutile type lattice, is not possible before the complete restructuring of the lattice, which slows down the process.[32s] The chemical reaction between the perovskite and TiO to form $CaTi_2O_4$ is also controlled by nucleation rather than the chemical reaction rate.[32s]

The debate over the reduction pathway and kinetics was perhaps because of some ambiguities in the data gathered from the ex situ characterization of the partially reduced sample, that is, analyzing the samples after cooling and washing. To avoid such ambiguity Bahgat et al.[34] used white beam synchrotron XRD to monitor in situ the phases change during the reduction of TiO_2. The in situ characterization made it clear that the reduction starts by converting TiO_2 to substoichiometric phases that improve the ionic conductivity of the oxide pellet.[34] This slight reduction in TiO_2 facilitates the transformation to nonstoichiometric $CaTiO_3$.[34] At the surface layer, $CaTiO_3$ reduces directly to Ti, while in the core of the pellet $CaTiO_3$ reacts chemically with TiO to form $CaTi_2O_4$. The $CaTi_2O_4$ is reduced to Ti by removing CaO.[34] The key difference between the ex-situ and in situ monitoring of TiO_2 electro-deoxidation in molten $CaCl_2$ under constant voltage condition are (1) Ti_4O_7 was the only Magnéli phase detected by the white beam synchrotron XRD. The phases Ti_3O_5, α-TiO and Ti_3O_2 were not observed, suggesting that these phases were formed by disproportionation reactions of Magnéli phases during cooling.[34] (2) In situ measurements proved that $CaTi_2O_4$ formed chemically by the coproportionation of TiO and $CaTiO_3$. (3) The in situ analysis suggests some removal of oxygen ions from the CaTiO3, which distort the crystal structure. This also suggests the long-ordered prisms detected for $CaTiO_3$ in the ex situ techniques were formed by the disproportionation of the nonstoichiometric $CaTiO_3$ to give TiO_{2-x} oxides and stoichiometric $CaTiO_3$.[34]

The electro-deoxidation of porous titanium dioxide pellets was studied under a controlled potential using a three-terminal cell. Typically the potential was ramped by 300 mV/h, and then dwelled at a constant potential ranging from −0.8 to −1.6 V.[32t] The current−time curve showed noticeable waves during the ramping stage, a peak at the start of the dwell stage, followed by a gradual decrease to a plateau background. Investigating the specimens taken at the waves by XRD and SEM analysis, revealed that titanium dioxide had been reduced to suboxides with the cogeneration of the perovskite phases, suggesting the same mechanisms depicted by eqs 22−26.[32t] However, the overall rate of the electro-deoxidation has increased significantly and it was possible to produce titanium powder with oxygen content as low as 2000 ppm under the conditions of depositing calcium.[32t]

The composition of the electrolyte and the presence of oxygen carrier ions play an important role in the electro-deoxidation mechanisms and also on the process rate. In the absence of oxide ions in the initial salt, calcium ions incorporated into the cathode must be associated with the chloride ions discharges at the anode to maintain the electroneutrality. Thus, it is not a surprise for chlorine gas to be evolved from the anode at total voltages far below 2.5 V. More importantly, the lack of carrier ions leads to a mass transfer limitation and consequently a longer reaction time.[32t] This is probably the reason for observing several Magnéli phases and other near-stoichiometric compounds after a relatively long time when applying the electro-deoxidation in a virtually oxide-free electrolyte.[19] Introducing an oxide to the melt facilitates the mobility of the oxygen ions and also makes the insertion of the calcium ion into the cathode more favorable from both the thermodynamic and kinetic points of view.[32t] However, at very high oxide concentrations the capability of the electrolyte to dissolve more oxygen ions decreases. Moreover, it increases the activity of CaO in the electrolyte, which tends to increase the possibility of depositing calcium metal or producing calcium ions with a lower oxidation state in the electrolyte, Ca^+ as an example, and leading to a drop in the current efficiency. At low calcium oxide levels, on the other hand, further reduction of phases like $CaTi_2O_4$ and $CaTiO_3$, was reported to be slow because of the depletion of the carrier anions before the decomposition of these calcium-containing intermediates. This depletion of oxide ions from the electrolyte is also possible at an initial oxide concentration up to 2 mol %, when the applied potential or voltage is high enough to decompose them, which was favored to produce low oxygen containing titanium. Hence, "to achieve rapid deoxidation of the cathode, it is of crucial importance that the majority of oxygen be removed at relatively low cathode potentials, i.e., when the calcium oxide concentration in the electrolyte is large, and that only small amounts of oxygen remain to be expelled at high cathode potentials, i.e., when the calcium oxide concentration in the electrolyte is diminished".[32t]

There are many developments addressed to achieve the aforementioned goal. Schwandt et al, slowly ramped the potential in the first stage of electrolysis so that most of the oxide content in the cathode was removed, before achieving the potential of depositing calcium, that is, before diminishing the concentration of the anions carriers in the electrolyte.[32t] Wu et al.[35] suggested that controlling the oxide content depletion in the electrolyte could be achieved by applying the cell voltage just required to achieve the cathodic potential needed to drive the reactions. In this technique, named the computer-aided control (CAC) method, the variation in the cell voltage was recorded during constant potential experiments and was used to apply a programmable constant voltage scheme.[35] At any point of the reduction, the cathodic potential was claimed to be

dx.doi.org/10.1021/cr200305x | Chem. Rev. 2013, 113, 2863−2886

constant as the applied voltage was determined from prior constant potential measurements.[35] Finally, Abdelkader et al injected a reducing agent locally near the cathode during the course of the reduction,[36] and it was found that calcium metal in a reasonable amount gives more driving force for the reduction.[36]

3.3.5. Zirconium Oxide. Zirconium is from the same transition metals group as titanium and they both have similar chemical and physical properties. With reference to the electro-deoxidation process, zirconium has two major differences. First, there is a range of room-temperature-stable Magnéli phases and suboxides in the Ti−O phase diagram, while the Zr−O system has only one nonstoichiometric compound reported, ZrO_{2-x} at high temperature. Second, CaO has limited solubility in TiO_2,[37] while the CaO forms a solid solution with ZrO_2 and stabilizes the high temperature cubic or tetragonal phases.[38] These two factors make the electro-deoxidation of ZrO_2 a very different process from the mechanistic and kinetic point of view when compared with TiO_2.

The results of analyzing partially reduced samples are confusing and might give an inaccurate reduction mechanism. That is because the nonstoichiometric oxides of zirconium disproportionate during cooling to give Zr and one of the stable zirconium oxides. Detection of some ZrO and ZrO_{2-x} by the XRD analysis in some cases might be due to the high carbon content of the cathode materials in these particular cases, which might stabilize these compounds.[36,39] Also, it could be attributed to the overlapping between ZrC and ZrO peaks.[36,39] Apart from those arguably existing compounds, there were only two intermediate phases confirmed by the XRD analysis: calcia stabilized zirconia CSZ[40] (given the general formula of $Ca_\alpha ZrO_\beta$ by Peng et al[41]), and calcium zirconate ($CaZrO_3$).[40] Reactions 27 and 28 summarized the proposed mechanism based on the ex-situ analysis. In-situ measurements, such as the synchrotron XRD technique, are necessary to determine the exact phase changes during the electro-deoxidation of ZrO_2. These are

$$ZrO_2 + \alpha Ca^{2+} + (4 - 2\beta + 2\alpha)e^- = Ca_\alpha ZrO_\beta + Zr + (2 - \beta)O^{2-} \quad (27)$$

$$Ca_\alpha ZrO_\beta + 2(\beta - \alpha)e^- = Zr + \beta O^{2-} + \alpha Ca^{2+} \quad (28)$$

Full reduction of pure ZrO_2 to metallic Zr was difficult to achieve under constant voltage. It was agreed that and all the attempts agreed that the reason could be explained by slow reaction kinetics. Li et al[42]obtained up to 93% zirconium recovery and explained the uncompleted reduction by the slow ionization of oxygen from the Zr−O solid solution. Mohandas and Fray[40] reported the reduction was blocked in the interior part of the pellet due to the dense morphology and high electrical resistivity of the generated $CaZrO_3$ and the initial ZrO_2. They also reported that the reduction improved by increasing the grain size of the initial ZrO_2 particles, and relate this to the increase in the diffusion rate of oxygen ions in the precursor zirconium oxide pellet, and also due to the decrease of the overall pellet resistance by diminishing the grain boundary area and intergranular pores.[40] The resistance of the generated $CaZrO_3$ was measured using a specially developed technique. This technique, based on interrupting the current circuit and measuring instantaneous voltage difference between the electrolytic and galvanic cell, is equal to *iR*.[43] The resistance of the ZrO_2 electrode increased during electro-deoxidation, attaining a peak value of 5.5Ω, as $CaZrO_3$ became the continuous phase.[43] It was then concluded, "electron-transfer reactions taking place at the cathode determine the rate and efficiency of the electro-deoxidation process to a great extent".[43]

3.3.6. Tungsten Oxide. Despite the debate on the effect of calcium doping of the initial oxide on the rate of electro-deoxidation, using calcium containing ternary compounds as starting materials, was necessary in some cases, to avoid undesired reactions between the cathode material and the electrolyte. During the electro-deoxidation of tungsten trioxide in molten $CaCl_2$ at 1173 K, a significant amount of WO_3 was lost because of the formation of the volatile tungsten oxychloride according to reaction 29.[44] Using $CaWO_4$ as a cathode precursor inhibited the formation of WO_2Cl_2, but conversely the high solubility of $CaWO_4$ in molten $CaCl_2$ (about 15 mol. % at 1173 K) imposed a restriction in $CaWO_4$ powder.[44] Decreasing the solubility of $CaWO_4$ was achieved by using a NaCl−$CaCl_2$ eutectic mixture at a lower temperature (873 K).[44] Calcium compounds significantly contaminated the produced powder and additional leaching with dilute HCl was necessary to isolate the tungsten powder.[44]

$$2WO_3 + CaCl_2 = CaWO_4 + WO_2Cl_2(g) \quad (29)$$

3.3.7. Aluminum Oxide. The formation of calcium aluminate intermediates was reported during the electro-deoxidation of solid Al_2O_3 cathode in $CaCl_2$-based molten electrolytes.[45] The attempts to electrodeoxidize Al_2O_3 in molten chloride bath is one of the earliest investigations of the FFC-process.[46] The early attempt met many obstacles due to the high electrical resistivity of Al_2O_3, the solubility of alumina in the chloride bath and loss of some aluminum in the electrolyte (since the produced metal is liquid at the operation temperature). Developments introduced to overcome these obstacles include using a mixed chloride system to decrease the solubility of Al_2O_3 in the electrolyte, and lowering the operating temperature to below the melting point of aluminum[47] and incorporation of Al,[45] or a readily reduced oxide powder[47b] into the starting oxide pellet in order to increase the electrical conductivity of the cathode.[45]

The intermediate phases formed during the course of the reduction depend strongly on the molten electrolyte. In a $CaCl_2$−LiCl melt, $Ca_{12}Al_{14}O_{33}$, $Ca_{12}Al_{14}O_{32}Cl_2$, and $LiAlO_2$ were detected as the ceramic phases before the materials electrodeoxidized, further to the aluminum rich Al−Ca alloys formed according to reactions 30−33, as suggested by Yan et al.[48] Upon using $CaCl_2$−NaCl, calcium aluminates were observed with no trace of sodium aluminate compounds.[48]

$$^{21}/_{2}Al_2O_3 + 12CaO + {}^{21}/_{2}C = 7Al + Ca_{12}Al_{14}O_{33} + {}^{21}/_{2}CO(g) \quad E^\circ_{1173K} = -0.962\ V \quad (30)$$

$$Ca_{12}Al_{14}O_{33} + 21C = 14Al + 12CaO + 21CO(g) \quad E^\circ_{1173K} = -1.222\ V \quad (31)$$

$$^{3}/_{2}Al_2O_3 + Li_2O + {}^{3}/_{2}C = Al + 2LiAlO_2 + {}^{3}/_{2}CO(g) \quad E^\circ_{1173K} = -0.701\ V \quad (32)$$

dx.doi.org/10.1021/cr200305x | *Chem. Rev.* 2013, 113, 2863−2886

$$2LiAlO_2 + 3C = 2Al + Li_2O + 3CO(g)$$
$$E^{\circ}_{1173K} = -1.352\ V \quad (33)$$

3.4. Electro-deoxidation of Mixed Oxides and Oxide Solid Solutions

This novel approach in the FFC-Cambridge process is based on driving out the nonmetallic component of the metal compound by applying an electrical potential. This approach enabled synthesis of many alloys and intermetallics by blending a mixture of the required element compounds, usually oxides, and to use it as cathode precursor. The process also introduced the principles for synthesis of new alloys with compositions that could not be achieved by the conventional smelting process. Most of the investigations into alloy synthesis were conducted under constant voltage conditions.

Niobium-based intermetallics superconductors were successfully produced at an early stage in development of the FFC process.[26a,49] Although the current−time curves for the production of intermetallics follow the typical curve reported for pure niobium production, the steady state current, which represents the ionization of oxygen atoms from the metal−oxygen solid solution, was obtained at an earlier time (3 h rather than 5 h in case of Nb_2O_5 reduction). NbTi and Nb_3Sn powder with oxygen content less than 180 and 4500 ppm, respectively, were formed. The produced materials exhibited the unique feature of superconductivity when the critical temperature determined in the AC susceptibility versus temperature curve was measured at a frequency of 333 Hz. Other niobium-based alloys that were synthesized via the electro-deoxidation process in molten $CaCl_2$ include: Nb−Si,[50] Nb−9Hf−Ti.[51] Ta−Nb,[52] Nb_3Al, and Nb_2Al.[53]

Alloys of titanium containing a beta-stabilized element have been successfully produced at a laboratory scale level. Homogeneous fine grains of hypo-eutectoid composition were prepared[14b,c,54] for the alloys: Ti-10 wt % Mo, Ti-10 wt % W, and Ti-10 wt % V. The microstructure of the three alloys was similar with pro-eutectoid α decorating grain boundaries, with the prior β grain interiors having transformed to eutectoid α/β structures.[14b,c,54b] Titanium dioxide was believed to have formed a solid solution with both the MoO_2 and V_2O_5 at the sintering step, giving the produced alloy a high degree of homogeneity.[14b] However, WO_3 does not form any solid solution with TiO_2, but it is reduced to WO_2 before the reduction of TiO_2.[14c,54b] At that point WO_2 will form a solid solution with TiO_2 prior to further reduction, which again gives the produced alloy a high degree of homogeneity.[14b]

Ferrotitanium and other titanium-base alloys were also prepared by the direct electro-deoxidation of the mixed oxide precursors.[55] Ma et al.[55a] used the naturally occurring ilmenite ore ($FeTiO_3$) to make the porous cathode in a two-terminal cell arrangement. The reduction started by forming pure iron and perovskite ($CaTiO_3$), which is subsequently reduced to Ti through intermediate steps of titanium suboxides.[55a] The Ti readily reacts with Fe to form the TiFe alloy.[55a] The same work reported the preparation of $TiFe_{0.4}Ni_{0.6}$ alloy by adding 4.46 wt % NiO to ilmenite in the initial precursor.[55a] Tan et al[55b] sintered a mixture of Fe_2O_3 and TiO_2 at 1373 K. The sintered pellet was a mixture of Fe_2TiO_5 and TiO_2, which then converted to a mixture of $CaTiO_3$, ilmenite ($FeTiO_3$), and a spinel phase (Fe_2TiO_4). Fe was the first metallic phase to appear, followed by the intermetallic Fe_2Ti, and finally the target compound FeTi.[55b] The same mechanism was also suggested by Guo et al.[56] LI et al[55c] prepared a series of different Fe−Ti alloys by changing the initial composition of the oxide mixture. They observed that for rich-Fe_2O_3 oxide mixtures, the products were mainly α-Fe and Fe_2Ti, while the product was Ti and FeTi when Fe_2O_3 was below 50 wt %.[55c] Liao et al mixed elemental Fe with TiO_2 with different stoichiometric ratios and obtained different compositions of the Ti−Fe alloy.[57] Other examples of titanium-base alloys or intermetallics prepared under a constant voltage mode, include Ti−6Al−4V,[58] Ti−45Al−9Nb,[59] Ti−Si,[60] Ti−29Nb−13Ta−4.6Zr,[61] Ti−Cr,[62]and Ti−Zr.[63]

Many attempts have been carried out to metallise the heavy rare earth oxides. Since the thermodynamic stability of such oxides are higher than that of CaO, it has been demonstrated that the electro-deoxidation of Tb_4O_7, Y_2O_3, and Dy_2O_3 is possible only under the conditions of Ca deposition, which leads to significant energy consumption.[64] Investigations were then focused on the production of functional intermetallic compounds for magnetic and energy applications. $TbFe_2$ and Tb_2Fe_{17} were prepared by the electrochemical reduction of Tb_4O_7−Fe_2O_3 solid solutions, thermally prepared during the sintering of the oxide mixture pellet at 1473 K.[65] The reduction was found to start by forming Fe, and then proceeded through the formation of various Tb−Fe intermetallic compounds to $TbFe_2$ (or Tb_2Fe_{17} depending on the initial oxides ratio). The produced intermetallic was cleaned by dimethylsulfoxide under magnetic stirring, leading to a pure magnetic powder with oxygen content of less than 1300 ppm.[65a] Production of $TbNi_5$ from NiO and Tb_4O_7, where there is no single phase between the oxides, was also reported.[65a] It was found that the reduction started by NiO being converted to Ni, and then followed by the thermal decomposition of Tb_4O_7 to Tb_2O_3, on the preformed Ni to form the intermetallic compound.[65a] Elemental Fe was used in the initial precursor to enhance the reduction of Dy_2O_3.[66] Forming the intermetallic $DyFe_2$ was reported to be thermodynamically possible at constant potential of 3.1 V, but was contaminated with $DyFe_3$ alloy and Dy_2O_3.[66,67]

Light rare earth oxides such as Nd_2O_3, CeO_2, and La_2O_3 have oxides less stable than CaO, but they react rapidly with the chloride melt to form oxychloride compounds prior to any electro-deoxidation reaction. Therefore, reducing these oxides through the FFC-Cambridge process in molten chloride bath was a challenge. One of the notable investigations to reduce light rare earth oxides was in the attempted preparation of $CeNi_5$ hydrogen storage intermetallics from a NiO−CeO_2 mixture.[68] It was claimed that the formation of the metallic phase is possible at 2.5 V in eutectic NaCl−$CaCl_2$, with the reduction pathway initiated by metallising NiO to Ni, which then reacts with CeOCl to produce $CeNi_5$.[68] Zaho et al[69] reported the preparation of $CeNi_5$ and $LaNi_5$ under 3.2 V in molten $CaCl_2$ at 1023 K. Zhang et al,[70] prepared $La_{0.5}Ce_{0.5}Ni_5$ using the same conditions and electrolyte. Song et al[71]used eutectic KCl−LiCl to produce $CeNi_4Cu$ alloy powders by electro-deoxidation of oxide precursors at 923 K. At such low temperature, no CeOCl was detected as an intermediate phase.[71] The oxygen content of the produced powder was about 0.5 wt.%.

The thermodynamic stability of the rare earth oxychlorides is not the only obstacle during the electroreduction of these compounds. The spontaneous reactions between the rare earth oxides and molten $CaCl_2$, and the associated fast changes from the hexagonal crystals of the oxides to the tetragonal structure of the oxychlorides destroy the integrity of the pellet. Chen et

dx.doi.org/10.1021/cr200305x | Chem. Rev. 2013, 113, 2863−2886

al[72] reported that the problem of maintaining pellet integrity was more significant when the two oxides completely dissolve in each other to form the phase $LaNiO_3$, and less severe when $LaNiO_3$ decomposed to NiO and $La_3Ni_2O_7$ by sintering the pellet in air at 1473 K for 2 h. The SEM images showed that the particles size increased from submicrometer to micrometre which strengthened the pellets.[72] Kang et al.[71] reported that the produced powder was contaminated by LaOCl even after 10 h of electrolysis at 3.1 V. Increasing the constant potential up to 3.5 V was reported to eliminate such undesired phases, although some lanthanum was lost in the electrolyte.[71]

The investigations carried out in the University of Cambridge revealed that the reduction mechanism during the formation of the light rare earth intermetallics is more complicated than just metallising Co or Ni, followed by reducing the rare earth oxides or oxychlorides. First, the electrical conductivity measurements for a pellet consisting of cobalt oxide and $NdCoO_3$, revealed that high ionic conductive materials facilitated the migration of oxygen ions inside the lattice.[73] Once the electric current was applied, Co ions in the center of the octahedral site are reduced, forcing the adjacent oxygen ions to be removed from the surface and create more oxygen vacancies.[73] The interaction between the salt and the cathode materials produced a single-phase compound of the form $NdCoO_xCl$.[73] Cobalt is then metallized from this phase, leaving the single cation phase, NdOCl, to react with the salt again to form $CaNd_2O_4$, with Nd ions being discharged as Nd onto the surface of the cathode.[73] In the final stage of reduction, $CaNd_2O_4$ was electro-deoxidized and after 10 h formed a mixture of Nd_2Co_{17} and $NdCo_5$, with there not being enough Nd in the cathodic material to form pure $NdCo_5$.[73] The deficiency in Nd is resolved by the deposited Nd from the salt diffusing into the intermetallic Nd_2Co_{17} alloy to form pure $NdCo_5$.[73]

Shape memory alloy formation with the FFC process has attracted much research work since the earlier stages of its development. The ferromagnetic shape memory alloy, Ni_2MnGa, that is capable of 5% strain in a magnetic field, was prepared from NiO and $MnO_2{\cdot}Ga_2O_3$.[74] When the assembled cathode was subjected to a 3 V constant voltage in molten calcium chloride, the resulted current−time curve started at 1.7 A and then dropped to a 0.3 A background current.[74] Subsequent examination of the produced material verified that this product had ferromagnetic and shape memory properties.[74]

Nitinol alloys, NiTi alloys, also received great attention because of their unique shape memory and pseudoelasticity properties, allowing them to be good candidates for many industrial and medical applications. First attempt to produce the binary alloy via the FFC-Cambridge process was introduced by Chen et al.[75] TiO_2 and NiO mixed oxide pellets, which form $NiTiO_3$ single phase compound after sintering at 1373 K, were cathodically polarized at 3.1 V against carbon anode.[75] The typical current−time curve showed three peaks in the first hour. The first peak was after 12 min with the current reaching near 2500 mA, which was associated with the reduction of NiO to Ni and the formation of $CaTiO_{3-x}$. The second peak was at 30 min, and the current was about 0.8 A, which was related to the start of titanium metallisation from the titanate phase forming Ni_3Ti.[75] The third peak after 1 h of electro-deoxidation was attributed to the complete metallization of the surface layer but, however, $CaTiO_{3-x}$ was still in the core of the pellet.[75] The slow propagation of the diffusion controlled titanate reduction in the interior of the pellet was clear from the gradual decrease in the current over the last 7 h.[75]

For a better understanding of the reduction mechanism, Dashwood et al[14a] controlled the raised rate of the voltage so that the current was maintained at around 0.5 A. This procedure ensures that there is sufficient time for the phase changes to take place.[14a] The results obtained clearly showed that reduction occurs through progressive layers. After the first 10 min the surface layer reduced to Ni surrounded by a $CaTiO_3$ matrix, while the core of the pellet maintained some of unreacted $NiTiO_3$.[14a] The only difference between this work and Chen's was the detection of Ni_2Ti_4O on the surface layer after 1 h of electro-deoxidation. This phase, coupled with other metallic phases, Ni, and Ni_3Ti, increased the porosity of the surface layer, and facilitated the reaction between $NiTiO_3$ at the core of the pellet with the salt, to form $CaTiO_3$, leading it to consolidate within the interior regions of the pellet.[14a] Three distinguishable layers were observed after 3 h of reduction: the Ni_2Ti_4O and $NiTiO_3$ on the surface; the $CaTiO_3$ and the Ni_3Ti in the middle; and the Ni and $CaTiO_3$ coexisting within the core. Both $NiTiO_3$ and metallic Ni gradually disappeared from the pellet, in favor of forming Ni_3Ti and the stoichiometric NiTi phase, after 6 h of electro-deoxidation.[14a] Over the remaining 24 h, the source of the intermetallic compounds was the reduction of Ni_2Ti_4O phase. The final composition of the alloy was a mixture of NiTi and Ti_2Ni.[14a] The later was initially attributed to the starting material being moderately Ti-rich. The authors then refined their justification by relating the formation of Ti_2Ni phase and monoclinic NiTi to the use of a Ti cathodic current collector that gave Ti enrichment.[76] That was further confirmed by using a Ni current collector in a constant potential experiment. The Ni enrichment stabilized the high temperature cubic crystal structure of NiTi down to the room temperature, and no Ti_2Ni was observed.[76] The electro-deoxidation of $TiNiO_3$ under constant voltage of 3.1 V was in situ studied using X-ray synchrotron diffraction. The general reduction pathway was somehow similar to that obtained from the ex-situ analysis.[77] However, Ni_3Ti was not observed in significant quantities "suggested that this is because Ni_3Ti observed in the ex situ studies is precipitated upon cooling due to the reduction of Ni solubility in NiTi at lower temperatures".[77]

Mg−Ni is another example of a nickel base intermetallic that was synthesized from their oxides via the electro-deoxidation process.[78] Surprisingly, sintering of a NiO−MgO mixture at 1473 K was not enough to form a single-phase solid solution.[78] The electroreduction proceeded by reducing Ni in the first step, and forming Mg−Ni intermetallic in the second step.[78] A significant amount of MgO was lost due to dissolution in the electrolyte. The Ni-rich intermetallic (such as $MgNi_2$) was obtained after applying a constant voltage at 3.2 V, for 24 h in molten $CaCl_2$−NaCl, at 1173 K.[78] The Mg-rich intermetallic (Mg_2Ni) is liquid at this temperature and therefore the electro-deoxidation was carried out at 978 K.[78] Only 18% of the sample was reduced to metallic phases.[78] It was only after applying 5 V that the sample completely converted to its metallic phases.[78] However, the obtained Mg_2Ni was contaminated by $MgNi_2$, $Mg(OH)_2$, and a small amount of residual MgO (5 wt.%).[78]

Zirconium-based alloys were recently prepared by the direct conversion of a porous cathode made of mixed oxides, in molten salt, under potentiostatic conditions. A well-consolidated tube of zircaloy (Zr-2.5Nb) was fabricated from tubular oxide precursors.[79] The electro-deoxidation was performed at a

dx.doi.org/10.1021/cr200305x | Chem. Rev. 2013, 113, 2863−2886

constant voltage of 3.1 V, for 48 h, at 1173 K, in molten $CaCl_2$.[79] Porous consolidate of (α+β)-TiZr and α-TiZr was also produced using the same conditions.[63] The proportion of the α- and β-phases was reported to be influenced by the oxygen content, and it was possible to adjust the required fraction of each phase by varying the electro-deoxidation time, and therefore eliminating the addition of any bioincompatible β-phase stabilizer.[63] AB2-type hydrogen storage alloys powder, $ZrCr_2$, $ZrCr_{0.7}Ni_{1.3}$, and $Zr_{0.5}Ti_{0.5}V_{0.5}Cr_{0.2}Ni_{1.3}$, were also synthesized at the same conditions of temperature and applied voltage.[80] The hydrogen storage capacities of the resulting powder was measured by a galvanostatic discharge−charge test, and exhibited much higher capacity than those reported in the literature for the powder prepared by arc-melting.[80]

3.5. Attempts to Use Inert Anode

For any electrochemical process, an inert anode is far more desirable than a consumable anode. The electro-deoxidation process in particular, where the raw material is usually an oxide (with other anions impurities accepted to a small extent), is expected to generate CO_2 and CO, and minor quantities of other greenhouse gases (CCl_4, C_2Cl_6) and sulphurous gases (SO_2, COS, CS_2, H_2S), if a carbon anode is used. The emission of these gases is not only unwelcome, but also results in rapid anode consumption. Also, the produced CO_2 dissolves in the melt forming carbonate ion CO_3^{2-} that can then react at the cathode, contaminating the produced metallic powder, according to reactions 34 and 35.[32s,81]

$$CO_2 + O^{2-} = CO_3^{2-} \quad (34)$$

$$CO_3^{2-} + 4e^- = 3O^{2-} + C \quad (35)$$

The idea of using an inert anode in the FFC-Cambridge process dates back to 2004, when British Titanium PLC and the University of Cambridge recognized that the process potentially offered another significant benefit, other than the cathodic production of metal. Molecular oxygen could be anodically synthesized instead of carbon oxides, if conventionally used graphite anodes were substituted by an inert anode. Indeed, it was conceived that the process could feasibly be used to anodically synthesize oxygen from regolith found on off-world sites, to ultimately refuel shuttles. Since oxygen is the significant reactant component (85 wt. %) for the propulsion of these rockets, locally produced oxygen from off-world regolith (consisting of a mixture of metal oxides), would ensure a greater economic viability of space travel to more distant regions of our solar system. Indeed, the FFC-Cambridge process was considered as a key component of the in situ resource utilization plans that were developed by NASA. Tripuraneni Kilby et al. used tin-oxide anode to extract oxygen from lunar regolith.[82] The selection of a tin oxide anode came after testing numerous metals, cermets (metal dispersed within a ceramic matrix), ceramics, and also carbon-based anodes.[83] The oxygen detected during electrolysis in the exhaust gas stream was significant when a tin oxide anode was used. A metallic product was also directly produced from JSC-1 (a lunar regolith stimulant material) using this anode material.[82,83]

NASA was not the only organization that expressed interest in using an inert anode with FFC-Cambridge process. ULCOS (ultralow carbon dioxide steelmaking) considered the production of iron through the electro-deoxidation of hematite, as a possible electrolysis route to reduce the carbon dioxide emissions if inert anodes were used. Motivated by this purpose, Burheim and Haarberg[84] tested nickel ferrite cermets containing excess nickel and copper as potential inert anodes in molten chloride baths. The anodes were thermally prepared from a mixing of NiO, Fe_3O_4, Cu, and Ni powder.[84b] The XRD and SEM analysis of the anode materials after electro-deoxidation, for 10 h at 923 K, showed that the surface was depleted of Ni and Cu. The anodes had a weight loss between 10 and 28 wt %.[84b] The dissolution of copper was found to be higher at a lower current density, and lower when the anode was pre-electrolyzed for long time.[84a] Increasing the temperature from 923 to 1123 K caused greater failure of the anodes.[84b]

Using carbon anodes is not only unfavorable from an environmental perspective, but it also leads to a decrease in the current efficiency. The parasitic reactions taking place in the electrolyte because of the dissolution of the carbon dioxide in the chloride melt also have a detrimental effect on the current efficiency. In addition, these parasitic reactions were reported to contaminate the cathodic product when the carbonate ion reduces to give carbon and oxygen ions.[85] Substituting carbon anodes with an inert anode eliminates the parasitic reactions and leads to significant improvement in the current efficiency. Tripuraneni Kilby et al.[86]reported a great improvement in the current efficiency when the graphite anode was substituted for a SnO_2-based material anode during the electro-deoxidation of chromium oxide. "For a 5.5 cm^2 anode surface area, the current efficiency was calculated to be 55% for the SnO_2-based material at 3 V; compared with 30% and 50% for graphite at 3 V and 2 V, respectively".[86] Similarly, upon using SnO_2-based anode in the electro-deoxidation of Ta_2O_5, the charge passed was 10300 C, while 17100 C being passed with a graphite anode.[87] Considering the theoretical charge required to reduce 1.9 g of Ta_2O_5 is 4423 C, then the current efficiency is 40% with the SnO_2-based anode and 24% with the graphite anode.[87] However, the reduction using a SnO_2-based anode is marginally slower when compared to the graphite anode reduction.[87] This may be due to the formation of an electrically resistive layer of calcium stannate ($CaSnO_3$) being formed on the surface of the SnO_2-based anode, which could inhibit electron transfer.[83,87] It could also be due to the higher potential required to discharge pure oxygen at the anode compared with carbon oxide generation using a graphite anode, which would reduce the potential available at the cathode.

Recently, a novel $CaRuO_3/CaTiO_3$ composite inert anode has been developed.[88] It was found that the electrical conductivity of calcium titanate ($CaTiO_3$) increased when doped (using solid state reactions at high temperature) with about 20 mol. % of $CaRuO_3$.[86] The conductivity of the composite anode increased further when nanosized $CaRuO_3$ was used as a doping agent, until 9 mol. %.[86] This nanosized $CaRuO_3$ was prepared by using reverse micelle synthesis.[89] The $CaRuO_3/CaTiO_3$ composite was tested as an inert anode in calcium chloride−calcium oxide melts, with a 4 g of titanium dioxide pellet used as a cathode.[88] The results showed the anode was still performing perfectly after 150 h of electro-deoxidation, with no sign of attack or decomposition.[88] Furthermore, a thin layer coating of the conductive $CaRuO_3/CaTiO_3$ solid solution was tested to introduce an economical alternative for the bulk composite.[88] Again no significant degradation was observed. The corrosion rate of the $CaRuO_3/CaTiO_3$ composite anode was found to be 1.5×10^{-3} g cm^{-2} h^{-1}, an order of magnitude less than that observed for SnO_2 in cryolite.[88]

dx.doi.org/10.1021/cr200305x | Chem. Rev. 2013, 113, 2863−2886

The performance of the $CaRuO_3/CaTiO_3$ composite anode was examined further during the production of NiTi shape memory alloys.[90] The molecular oxygen produced on the inert anode was recorded with a stabilized zirconia oxygen sensor continuously during electro-deoxidation. The variation of oxygen was in accordance with the trend of the analogous current versus time profiles confirming that reaction 6 is the anodic reaction[90] and suggesting that the oxygen generated was from the cathodic oxide and produced through the electro-deoxidation process.

Also, the anodic potentials on the carbon and $CaTiO_3/CaRuO_3$ anodes were measured during the electro-deoxidation with a reference electrode. Theoretically, the difference between the liberation potentials of O_2 on an inert anode, and CO_2 on a graphite anode, according to reactions 6 and 4, respectively, should be 1 V (1.6 V for CO_2 and 2.62 V for O_2 versus Ca^{2+}/Ca). However, the obtained results showed that the potential on the $CaTiO_3/CaRuO_3$ anode is only 0.4 V higher than that on the graphite anode (1.6 and 1.2 V versus a Mo reference, respectively).[90] This result was due to the overpotential required for the liberation of O_2 on the $CaTiO_3/CaRuO_3$ anode being much lower than that required for the liberation of CO_2 on the carbon anode. Furthermore, it was concluded that the oxygen evolution on the $CaTiO_3/CaRuO_3$ material is kinetically more favorable than the generation of carbon oxides gases on carbon and may partially offset the theoretical 1 V lower cell operation capability of graphite anodes compared with oxygen evolving anodes for the electro-deoxidation process.[90]

The corrosiveness of the chloride bath, and the interaction between the chloride ions and the anode materials are believed to be responsible to a great extent for the anode dissolution. Cox and Fray[91] used a less corrosive electrolyte, sodium hydroxide, and nickel wire as an inert anode. The anode was stable for 140 h because of the formation of thin oxide film composed mainly of Ni_2O_3 with traces of NiO_2.[91a,b] The main issue arose from using NaOH, and from the instability caused by the dissolved water. The activity of the dissolved water in the NaOH is increased by reaction 36, which is taking place spontaneously when the pellet is immersed in the salt. Increasing the activity of water in the melt lowers its decomposition potential to 1 V, which makes the evolution of hydrogen the favored reaction, and consequently reduces the current efficiency. Adding 1 wt % sodium oxide to the melt reduces the activity of water in the melt, increasing the decomposition potential to 1.6 V, which favors the reduction of Fe_2O_3 and raises the current efficiency from 32% to 89%. The overall cell reactions are[91a,b]

$$Fe_2O_3 + 2NaOH = 2NaFeO_2 + H_2O_{(inthemelt)} \quad (36)$$

cathode

$$Fe_2O_3 + 6e^- = 2Fe + 3O^{2-} \quad (37)$$

$$2NaFeO_2 + 6e^- = 2Fe + 3O^{2-} + Na_2O \quad (38)$$

in the melt

$$3O^{2-} + 3H_2O = 6OH^- \quad (39)$$

anode

$$OH^- = 3H_2O + {}^3/_2O_2 + 6e^- \quad (40)$$

overall reaction

$$Fe_2O_3 = 2Fe + {}^3/_2O_2 \quad (41)$$

4. CYCLIC VOLTAMMETRY

Cyclic voltammetry (CV) has gained great popularity in investigating the kinetics and understanding the mechanisms of the electro-deoxidation process. For this potentiodynamic technique, a potentiostat is used to ramp the potential with a constant scan rate ν (given in V/s) from potential E_1 to potential E_2 and back to E_1.[92] In the context of the electro-deoxidation process, cyclic voltammetry has many advantages that can help to gain an insight into the electrochemical behavior of the oxide being studied, and its interactions with the electrolyte. First, the ability of varying the scan rate makes CV applicable to study electrode processes even when the products or intermediates are very short-lived ($<10\ s^{-1}$).[93] It is also possible through CV to obtain data about the thermodynamic parameters of the process or species being studied, such as the redox potential.[94] Also, CV is a strong technique to detect surface processes like adsorption and oxide layer reduction. A major advantage of CV is that it provides direct insights into the kinetics of electrode reactions, which includes both heterogeneous and homogeneous electron-transfer steps, as well as coupled chemical reactions. Furthermore, CV gives a good idea of any complex side processes, such as pre- and postelectron transfer reactions.[95]

4.1. Understanding the Cathodic Reduction Reactions

The first attempt to use CV to determine the electro-deoxidation pathway by recording the intermediate phases was carried out by the inventors of the FFC-Cambridge process. Fray et al. carried out cyclic voltammetry experiments with an oxide-coated titanium foil as the working electrode, in molten calcium chloride at 800−1173 K.[96] The voltammograms obtained (Figure 2), clarified that the cathodic branch of

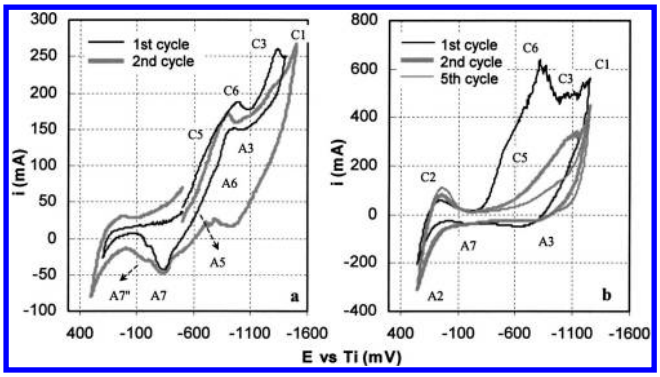

Figure 2. Cyclic voltammograms of oxide scale-coated Ti foils in molten $CaCl_2$ (a) at 1073 K with the sample prepared by heating in air at 973 K for 336 h and (b) at 1173 K with the sample prepared by heating in air at 973 K for 40 h (versus a Ti quasireference).[96] Reprinted with permission from ref 96. Copyright 2002 the Electrochemical Society.

the CVs involves three steps for removing oxygen: two from the oxide phase (C5 and C6) and one from the metal phase (C3).[96] Using thermodynamic calculations, the following reactions were proposed to account for these peaks:

$$C_6 \quad TiO + 2e^- = Ti + O^{2-} \quad (42)$$

dx.doi.org/10.1021/cr200305x | Chem. Rev. 2013, 113, 2863−2886

$$C_5 \quad 2TiO_2 + 2e^- = Ti_2O_3 + O^{2-} \tag{43}$$

$$Ti_2O_3 = TiO_2 + TiO \tag{44}$$

C3 is the ionization of oxygen from the Ti surface, and A7 is the reoxidation of titanates phase.

The titanate phase was assumed to be formed by the reaction of titanium oxide and CaO,[96] which is always present in $CaCl_2$. It was believed that CaO was formed, when the discharge of oxygen anions from the oxide phase into the molten salt was sufficiently fast to cause saturation of CaO, which then reacts with the partially reduced oxide scale to form the calcium titanates.[96]

Another voltammetric study to investigate the intermediate phases formed during the electro-deoxidation of TiO_2 on molten $CaCl_2$, was carried out using 10 μm oxide films thermally formed on a titanium rod at 973 K.[97] By increasing the potential limit in the positive direction, two initial reduction peaks were observed occurring at potentials 300 mV negative of the open circuit potential (C3 and C4 in Figure 3). The XRD

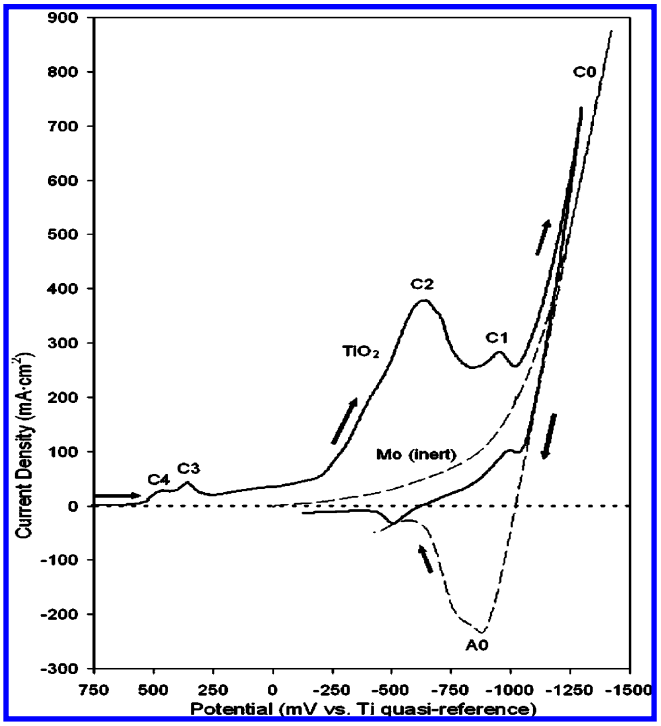

Figure 3. CV of oxide scale-coated Ti foils and an inert electrode in $CaCl_2$ at 1173 K (50 mV/s).[97] Reprinted with permission from ref 97. Copyright 2005 the Electrochemical Society.

analysis showed that the material produced at the first peak was a mixture of Ti_2O_3, Ti_3O_5, and $CaTiO_3$ and hence these peaks were ascertained to be the reduction of TiO_2 to Ti_3O_5, and the disproportion of the latter to Ti_2O_3 and TiO_2 (reactions 45 and 46). At the second peak, the XRD patterns indicate no Ti_3O_5 but a significant quantity of $CaTiO_3$ and Ti_2O_3, and hence, this peak was related to the conversion of Ti_3O_5 to Ti_2O_3 via reaction 47. The titanate phase was attributed to be formed via a precipitation reaction between Ca^{2+} and the remaining TiO_2 (reaction 48). Peak C2 was proposed to be for the reduction of Ti_2O_3 or $CaTiO_3$, to TiO, via reaction 49 and 50. Finally, peak C1 was related to the end of the reduction pathway by converting the produced TiO, from the previous step, to Ti via reaction 51.

$$C4 \quad 3TiO_2 + 2e^- = Ti_3O_5 + O^{2-} \tag{45}$$

$$Ti_3O_5 = Ti_2O_3 + TiO_2 \tag{46}$$

$$C3 \quad Ti_3O_5 + 2e^- = Ti_2O_3 + O^{2-} \tag{47}$$

$$TiO_2 + Ca^{2+} + O^{2-} = CaTiO_3 \tag{48}$$

$$C2 \quad CaTiO_3 + 2e^- = Ca^{2+} + O^{2-} + TiO \tag{49}$$

$$C2 \quad Ti_2O_3 + 2e^- = 2TiO + O^{2-} \tag{50}$$

$$C1 \quad TiO + 2e^- = Ti + O^{2-} \tag{51}$$

The intermediate phases observed during the electro-deoxidation of chromium sesquioxide (eqs 20 and 21) was further confirmed by CV.[98] The chromium oxide powder was manually filled into 0.3−1.0 mm diameter holes drilled in a molybdenum foil. This assemblage, named metallic cavity electrodes MCEs (Figure 4a and b), aimed to decrease the *iR* drop and consequently enhance the sensitivity of the CV measurements by using small amounts of powder.[98] The cyclic voltammograms obtained (Figure 4c−f) showed an irreversible reduction current peak, diminishing gradually after the first cycle. This peak was preceded by a current shoulder, or a long

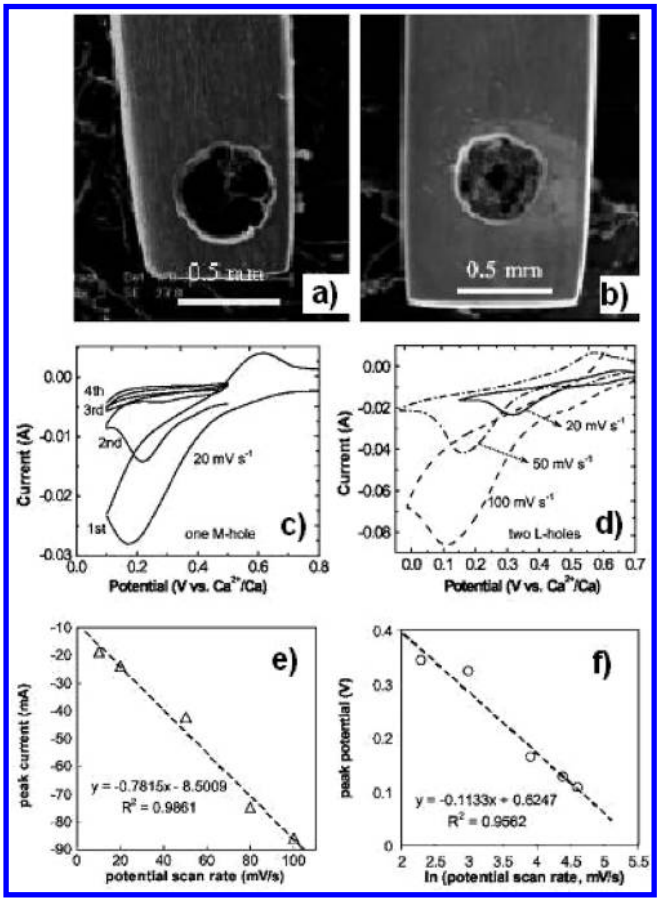

Figure 4. (a) SEM image of an empty MCE, (b) SEM image after filling the MCE with the oxide powder, (c) CV of Cr_2O_3 filled MCE for different cycles measured at 20 mV/s, (d) CV of Cr_2O_3 filled MCE at different scanning rates, and (e and f) linear correlations between the peak current and scan rate and between the peak potential and logarithm of scan rate respectively.[98] Reprinted with permission from ref 98. Copyright 2005 the Electrochemical Society.

dx.doi.org/10.1021/cr200305x | *Chem. Rev.* 2013, 113, 2863−2886

prepeak period, in which the current was greater than the background level.[98] The authors referred this significant current peak to the irreversible reduction of the oxide, and the prepeak shoulder to the formation of the chromite phase in a process similar to that represented by eq 48. The gradual diminishing of the current peak and shoulder indicates a fast electron transfer process for the small amount of oxide in the metal cavity, which might not be the case for a larger pellet.[98]

Niobium pentoxide is another example in which CV was used to study the reduction pathway. About 1 mg of Nb_2O_5 was manually pressed in a 0.5 mm hole, for a metallic cavity electrode similar to that used with chromium oxide.[99] The cyclic voltammograms (Figure 5) shows 6 reduction peaks

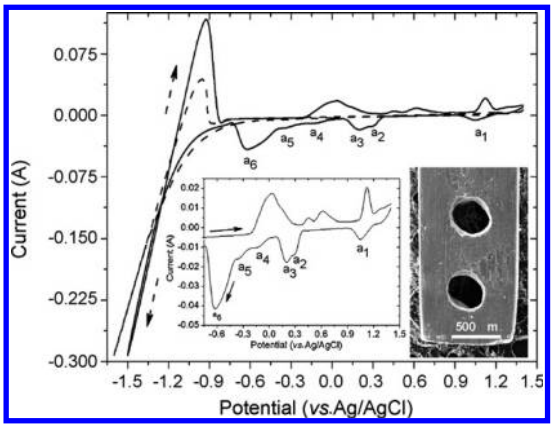

Figure 5. CV of empty (dashed line) and Nb_2O_5 filled MCE (sold line) recorded at 50 mV/s.[99] Reprinted with permission from ref 99. Copyright 2008 Elsevier.

before the deposition of calcium.[99] The first reduction peak a1 was associated by the formation of NbO_2, $CaNb_2O_6$, and $Ca_3Nb_2O_8$.[99] The reduction current decreased to a background level, indicating no reduction. The XRD pattern of the sample taken at a potential between a1 and a2 suggests $Ca_3Nb_2O_8$ was completely converted to $CaNb_2O_6$. Further electro-deoxidation was achieved by forcing the system toward more negative potentials, that is, toward the two conjunction peaks a2 and a3. At that point NbO_2 and $CaNb_2O_6$ were reduced to NbO and $Ca_{0.95}Nb_3O_6$. At a4, the predominant phases were $Ca_{0.95}Nb_3O_6$, $CaNbO_3$, and Nb with a small amount of NbO, and this suggests metallic niobium was formed mainly from the reduction of NbO. The last two reduction peaks overlapped and the reduction product for both of them was mainly metallic niobium, indicating that $Ca_{0.95}Nb_3O_6$ and $CaNbO_3$ had been reduced directly to metallic niobium. However, the authors deduced that $CaNbO_3$ needed fewer electrons to be reduced, and then, they concluded that peak a5 represents the reduction of $CaNbO_3$, while peak a6 is the reduction of $Ca_{0.95}Nb_3O_6$.[99]

There was an attempt to understand the mechanism of uranium oxide reduction in molten Li_2O–LiCl by using CV. The standard potential difference between the deposition of Li and the direct reduction of U^{4+} (0.15 V) made it difficult to distinguish whether the conversion of UO_2 to metallic uranium proceeded through the ionization of oxygen or by chemical reaction between the UO_2 and the deposited Li.[100] Careful examination with a CV of a nickel basket containing crushed UO_2 pellets (Figure 6 a and b) showed a small reduction current peak, although not discussed by the authors, at about 0.15 V more positive than Li deposition.[101] This peak and its associated reduction peak can also be detected in the second cycle, indicating the direct reduction of UO_2 might also be considered.[101]

4.2. Determining the Optimum Operation Potential

Cyclic voltammetry has been used to determine some thermodynamic parameters of the electro-deoxidation process and subsequently to optimize the production operation conditions. An example is the conversion of quartz to silicon in molten $CaCl_2$. The cyclic voltammetry experiments (Figure 7) showed two reduction–oxidation pair of peaks, at around 0.4 and 1.3 V versus Ca^{2+}/Ca.[102] The cathodic and anodic current observed at 1.3 V corresponded to the reduction of SiO_2 and the oxidation of Si, while the pair of peaks observed at 0.4 V was related to the formation and dissolution of calcium from Si–Ca.[102] Similar results were obtained from a porous SiO_2 pellet and a dense SiO_2 plate in a LiCl–KCl–$CaCl_2$ molten salt but with a slightly anodic shift of the peaks position[103] and also with more peaks corresponding to several intermetallic compounds in the form Si_xM_y.[104] On the basis of this data, a constant potential was applied between the SiO_2 plate and a carbon counter electrode at 1 V (versus Ca^{2+}/Ca).[105] After 2 h of the electro-deoxidation, the whole surface of the plate changed to dark color of crystalline silicon, while the core of the sample remained as SiO_2. Although the whole SiO_2 plate is expected to be reduced to silicon by an extension of the electrolysis time, a heat treatment method was tested to separate silicon from SiO_2. Melting the samples under vacuum at 1773 K, and using the following solidification process enabled the formation of a silicon ingot with 99.80 at % purity.[105]

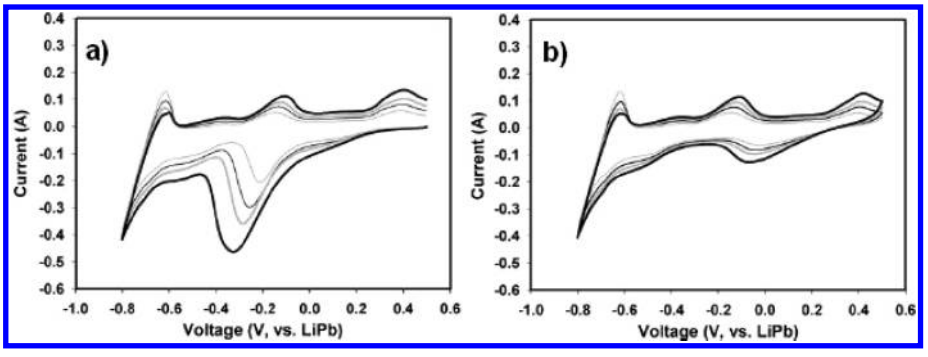

Figure 6. CV of a nickel basket filled with crushed UO_2 pellet in molten LICl at different scan rates ranging from 100 mV/s (light-thin line) to 250 mV/s (solid-bold line) for (a) the first cycle and (b) the second cycle.[101] Reprinted with permission from ref 101. Copyright 2010 Elsevier.

dx.doi.org/10.1021/cr200305x | *Chem. Rev.* 2013, 113, 2863–2886

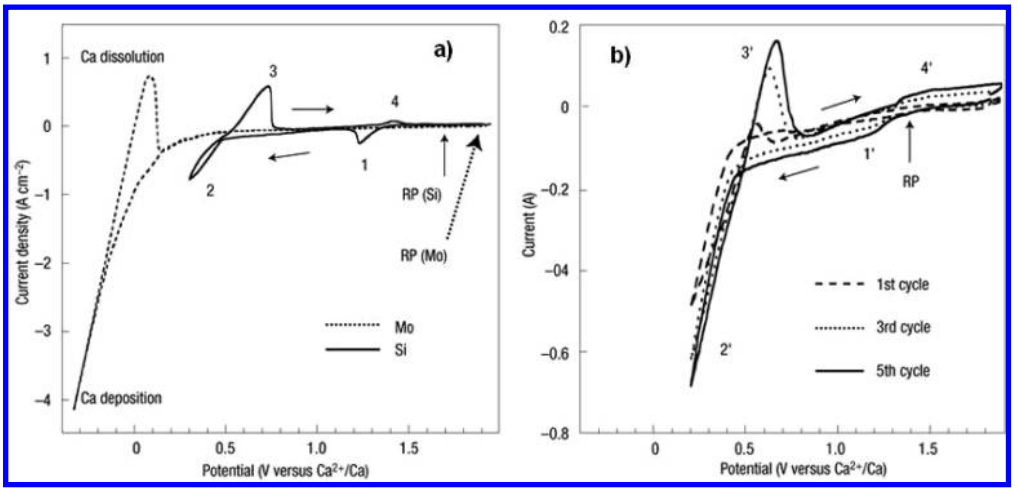

Figure 7. CV of a Mo wire and (a) single-crystal Si plate and (b) quartz plate in molten $CaCl_2$ at 1123 K measured at 20 mV/s.[102] Reprinted by permission from reference 102. Copyright 2003 Macmillan Publishers Ltd.: *Nature Materials*.

4.3. Exploring the Surface Phenomenon

The application of CV in investigating the surface phenomenon during the electro-deoxidation was mainly devoted to verify the thin layer 3PIs model. The CV was conducted in molten $CaCl_2$ at 1173 K, using the graphite crucible as the counter electrode, and Ag/AgCl reference electrode. The working electrode was a tungsten wire sealed in a quartz tube (~300 μm diameter).[24b,106] It is expected from the thin layer 3PIs model that the propagation along the surface should be controlled by charge transfer, because the discharged O^{2-} can readily enter the nearby molten salt. The CV recorded between −0.6 to −0.9 V was almost linear with a higher current in the reverse cycle than the forward one; suggesting that the process in this range is electron transfer with no diffusion limited steps involved. The CV also recorded an increase in current with potential in the same cycle, and increase in the overall current after every cycle, which proved the continuous expansion of the circular Si/SiO_2/electrolyte 3PI with both potential and time, as predicted from the mathematical representation of the thin 3PIs model.[24b]

Another example of using CV for studying surface phenomena can be obtained from the CV of UO_2 in molten LiCl−1 wt.% Li_2O at 923 K. The CV showed a peak before the deposition of Li. This peak disappeared after the first scan cycle (Figure 6b), which means it cannot be related to the direct reduction of UO_2, as bulk uranium oxide was used in the experiments[101] This peak was attributed to the under-potential deposition of Li on uranium oxides due to the energetically stable formation of a Li monolayer on the UO_2 surface.[101]

4.4. Studying the Complex Side Processes and Detecting the High Temperature Intermediate Phases

Comparing the electrochemical windows of a nonredox electrode, such as carbon, with the cyclic voltammograms of oxides in the same electrolyte gives a good idea about the complex pre- and postpeak processes. It is well-known that for a process confined in the electrode, the background current approaches zero in the absence of redox active species on the electrode and slow Faradaic surface transformation processes.[92] In agreement with this, the observed prepeak current of a glassy carbon working electrode in molten CaO−$CaCl_2$, and a graphite electrode in molten $CaCl_2$ and molten LiCl−KCl−$CaCl_2$ were almost zero.[107] In contrast, the current after the SiO_2 reduction peak in molten $CaCl_2$ was not zero and gradually increased until the potential reached the peak of the Ca−Si alloy formation (Figure 7b),[24d,102,103] suggesting a process that takes place slowly and over a wide range of potentials. This CV finding opened the door for further investigations of the processes between the two reduction peaks. The SEM image for the sample obtained at a potential of 0.70 V versus Ca^{2+}/Ca (Figure 8) showed many cavities on the

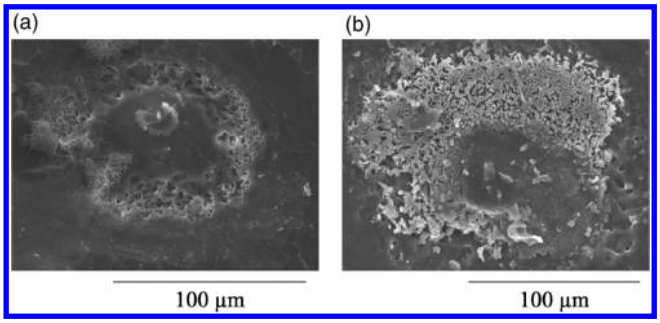

Figure 8. SEM images of the reaction interface for the SiO_2 plate obtained by pinpoint reduction at 0.70 V for (a) 1 and (b) 2 s in molten $CaCl_2$ at 1123 K.[103b] Reprinted with permission from ref 103b. Copyright 2007 The Electrochemical Society.

SiO_2 plate surface, which resulted from the dissolution of the silica in the melt according to eq 52.[103b] Moreover, this silica dissolution takes place after the concentration of the oxygen ions in the SiO_2 surface increased because of the direct reduction of SiO_2 to silicon.[103b] "When pO^{2-} and $a_{SiO_3^{2-}}$ reach 5.2 and 2.12 × 10^{-2}, respectively, solid $CaSiO_3$ is formed on the SiO_2 surface. Then, the reduction of SiO_2 to silicon proceeds via a formation of solid $CaSiO_3$ intermediate"[103b] via eqs 53 and 55. This dissolution-interaction mechanism is expected to be slow, which explains the slow change of the baseline current after the SiO_2 reduction peak. Moreover, the anodic and cathodic current increases with the number of cycles,[102] while the rate of change of the pre- and after-peaks current with the potential within the same cycle was almost constant, suggesting an enlargement of the reaction area.

$$SiO_2(s) + O^{2-} = SiO_3^{2-} \quad (52)$$

$$SiO_2(s) + CaO(l) = CaSiO_3(l) \quad (53)$$

dx.doi.org/10.1021/cr200305x | *Chem. Rev.* 2013, 113, 2863−2886

$$SiO_2(s) + CaO(l) = CaSiO_3(s) \quad (54)$$

$$CaSiO_3(s) + 4e^- = Si(s) + Ca^{2+} + 3O^{2-} \quad (55)$$

In contrast, the cyclic voltammogram of ZrO_2 powder filled within a metallic cavity electrode (Figure 9) showed a small current plateau prior to the first reduction peak.[108] This plateau was not observed in the electrochemical window of an empty MCE in the same electrolyte, suggesting a slow electrochemical process on the ZrO_2 powder,[108] and likely was due to the interaction of the oxide with the calcium ions. Although a perovskite zirconium phase is present in the ZrO_2−CaO system and has been reported through the electro-deoxidation of porous ZrO_2 pellets,[36,109] the EDX analysis did not detect any calcium-containing phase from the powder in the MCE.[108] This discrepancy was attributed to the difficulty of trapping O^{2-} ions in the MCE, which coupling with Ca^{2+} ions, could form the perovskite chemical phase similar to reaction 48.[108] Furthermore, the absence of stable Zr(III) and Zr(II) states in the Zr−O phase diagram[110] does not support an electrochemical partial reduction route similar to that represented by eqs 45−51.[108] However, there is no thermodynamic or kinetic reason to exclude the formation of the unstable-nonstoichiometric phases of zirconium oxides under the reduced condition provided in the electro-deoxidation process. These phases are difficult to be detected by EDX or XRD analysis as they are not stable in the normal atmosphere and also as it might oxidize easily during the washing step. However, it might be detected by a simultaneous technique such as CV.

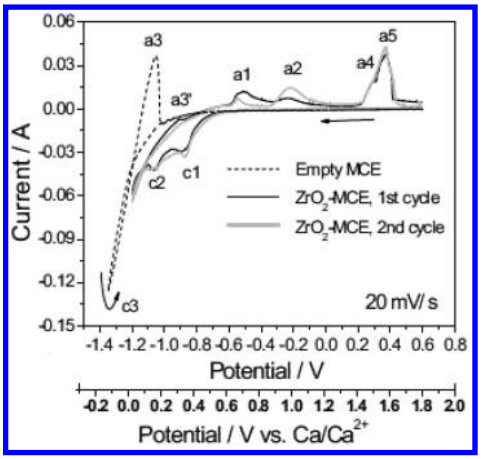

Figure 9. CVs in molten $CaCl_2$ at 1173 K for the empty (dashed line) and ZrO_2 filled (black line, first cycle; gray line, second cycle) MCE.[108] Reprinted with permission from ref 108. Copyright 2010 The Electrochemical Society].

4.5. Providing Direct Insights into the Kinetics of Electrode Reactions

The overall rate of the electro-deoxidation process is usually determined by the slow deoxidation of the metal−oxygen solid solution formed at the last stage of the process. Studying the kinetics of this diffusion-controlled step by CV is probably inappropriate. However, the CV gives an insight about the kinetic of the reactions that take place prior to the formation of the metal phase. Examples include confirming the slow 3PIs propagation in the core of the pellet, the reduction of metastable compounds observed during the reduction of ZrO_2 and the fast reduction of solid Ta_2O_5. Furthermore, the data obtained from CV was used to develop models to calculate the diffusion coefficients of oxygen in titanium oxides.

The reduction of pure zirconium dioxide was reported to be thermodynamically possible but kinetically slow.[36,109] The reason was, however, ambiguous. From reference to CV of 0.5 mg ZrO_2 powder filled in a metallic cavity electrode (Figure 9), it was revealed only 33% of the theoretical charge had been passed after the first cathodic potential scan.[108] This incomplete reduction was attributed to the following reasons: (1) the poor conductivity of ZrO_2 at the experimental temperature that makes the reduction proceed only through the inhomogeneous and slower propagation of the metal|ZrO_2|electrolyte interlines and (2) the large particle size of the zirconia powder used in this study (up to 10 μm).

There is some evidence from CV that supports these explanations. For the first explanation, although the conductive intermediate Zr_xO ($x \geq 1$) phase was observed after the first reduction peak, the CV showed a diminutive current shoulder over a long potential range. This shoulder represents a very electrochemically inert phase as the current was almost constant. The second explanation finds some support from the CV of the Zr wire, with or without a thick oxide layer, where the particle size is small, and the recorded reduction peaks are much larger.

The dynamic of the 3PIs propagation and the double layer effect have also been studied by CV. A silica sheathed tungsten disc was used as the working electrode in molten $CaCl_2$ at 1173 K.[106] The cyclic voltammogram exhibited two peaks for the reduction of SiO_2, and the formation of Ca−Si alloys as discussed earlier. The reduction current in the forward scan was higher than that in the reverse scan for the first cycle, and vice versa for the following cycles. This behavior was attributed to the increase of the double-layer current influence as the Si/SiO_2/$CaCl_2$ 3PIs developed in both the transverse and depth directions.[106] The double-layer effect was further studied by changing the scan rate, and was proved to have an unusually voltammetric feature with the current reducing with a decreasing scan rate. This unique phenomenon was explained by the 3PI model.[106] At a lower scan rate, the reduction of SiO_2 takes place over a longer time than in the fast scan, producing a longer 3PI length at the same potential and consequently a greater current.[106]

Assuming the reduction of the silica in the composite SiO_2/W electrode is a charge transfer process, a sphere of radius r and surface area S should result from the Si/SiO_2/$CaCl_2$ 3PIs symmetrical propagation. Also, the reduction current I, should be proportional to S, and to the apparent exchange current density i^o, according to eq 56, and at a large overpotential η, it should also be proportionate to the total charge of the reduction Q and the scan rate ν, according to eqs 57:[106]

$$I = i^{\circ} S \exp\left(\frac{\alpha n F \eta}{RT}\right) \quad (56)$$

$$I = i^{\circ} k_2 Q^{2/3} \exp\left(\frac{\alpha n F \nu t}{RT}\right) \quad (57)$$

Equation 56 predicts an exponential relation between current and potential. However, upon representing the part of the negative scan between the two reduction peaks, the current changed linearly with the potential, indicating the process is not only controlled by charge transfer.[106] Furthermore, a representation of the logarithmic current taken at certain charges showed a logarithmic linear relation with the scan rate.

dx.doi.org/10.1021/cr200305x | Chem. Rev. 2013, 113, 2863−2886

The slope of the line was about 0.5, which is closer to that of a mass transfer process, and deviated significantly from that predicted by eq 57 for a charge transfer processes at constant Q (slope of 1.0). In other words, the finding of the CV proved that the process is partially mass diffusion controlled and partially charge transfer controlled.[106] A good explanation might come from the 3PIs model, which as discussed previously, predicts the reaction to proceed through the thin layer (T3PIs) model on the surface, and the penetration (P3PIs) model on the depth direction. "The 3PI propagation along the surface should be controlled by charge transfer because the discharged O^{2-} can enter the nearby molten salt quickly. However, the O^{2-} ions resulting from the 3PI penetration into the solid have to move firstly through the reduction-generated porous Si layer. Consequently, diffusion would become more influential when the silicon layer grew thicker with the progress of the reduction."[106]

The reduction of solid Ta_2O_5 was studied by oxidizing a Ta wire in air for time ranged between 5 and 10 s at 1133 K.[30] The recorded CVs for the Ta_2O_5 coated wire showed three reduction peaks, and the current of them increased by increasing the Ta_2O_5 coating thickness. However, the anodic part and the second scan cycle of all the samples were similar, despite the thickness of the coating providing evidence that the reduction was very fast and was completed in the first negative scan even with a large quantity of Ta_2O_5.[30]

The recorded CVs of TiO_2 reduction[13,32d,111] were used to verify a model that can calculate some kinetic parameters, such as diffusion coefficients for oxygen in the various oxide phases of titanium, and the symmetry factors in the kinetics equation. A good fit was obtained between the resembled voltammogram and the experimentally recorded one by assuming a first order reaction. The model determined the diffusion coefficients for oxygen in for Ti_2O_3 and Ti_3O_5, to be 9.14×10^{-9} and 8.24×10^{-9} cm^2 s^{-1}, respectively. The values of the exchange current densities for the transformation of TiO_2 to Ti_3O_5 and Ti_3O_5 to Ti_2O_3 were estimated to be 0.0289 and 0.0856 A/cm^2, respectively. The cathodic transfer coefficients were determined to be 1.99 for the same transformation reactions.

5. ELECTRO-DEOXIDATION UNDER CONSTANT CURRENT CHRONOPOTENTIOMETRY

The principles of electrolysis at constant current has been known since 1900.[112] Unlike chronoamperometry and cyclic voltammetry where the potential is controlled as the independent variable, while the current is the dependent variable, chronopotentiometry (CP) controls the current and records the potential as the dependent variable. The steady current applied to a working electrode immersed in quiescent solution causes the lowest potential redox step to take place, and the potential of the electrode moves to values characteristic of the couple, and varies with time as the concentration of the ion ratio changes at the electrode surface. When the concentration of the ion under consideration drops to zero at the electrode surface, the potential will then rapidly shift toward higher values until a new, second redox process can start.[92] The point at which the concentration of ions in the vicinity of the working electrode approaches zero, is called the transition time τ. Sand's equation (eq 58) describes the transition time as a function of the electroactive species concentration C and current density i for a diffusion controlled process in an unstirred electrolyte.[113]

$$\tau^{1/2} = \frac{\pi^{1/2} nFAD^{1/2} C^b}{2i} \tag{58}$$

The shape of the chronopotentiogram for a Nernstian process is given by eq 59[113,114]

$$E = E_{\tau/4} + \frac{RT}{nF} \ln \frac{\tau^{1/2} - t^{1/2}}{t^{1/2}} \tag{59}$$

where the quarter wave potential ($E_{\tau/4}$) is the point on the curve when the logarithmic term becomes zero, that is, the potential when $t = \tau/4$.

Equation 59 applies to reversible charge transfer systems, Ox + ne = Red, with all the redox species being soluble in the electrolyte.[113,114] In the electro-deoxidation of the metal oxide, the products are the oxygen ions, and the molten electrolyte must have the ability to dissolve and transport these oxygen ions, making eq 58 and 59 valid under a moderate current density. However, noticeable deviations from the simple theory are expected at a high current density (short transition times) because of the two main reasons: charging of the capacitance of the electrical double layer may consume an appreciable fraction of the applied current and roughness of the solid oxide electrodes may cause the current density to vary over the surface.[115] Another disadvantage of the CP technique, in the context of the electro-deoxidation process, is the weak driving force to ionize the oxygen atoms from the generated solid metal, which makes CP only limited to certain metals and alloys that have low oxygen solubility. The lack of the oxygen ions supplied at the electrode surface will shift the electrode potential in a negative direction, until some other redox reaction (including the decomposition of the electrolyte) can take place to maintain the constant current.

CP has, however, many advantages that might favor it for the electro-deoxidation process. CP is simple, and needs less construction and operation considerations. Another advantage of CP is that the ohmic drop resulting from solution resistance is also constant because it is equal to the product of the current and the solution resistance. The ohmic distortion can therefore be simply corrected by a constant potential offset, allowing greater control of the process. In contrast, in potentiostatic experiments, the current, and hence the ohmic drop, varies with potential, and the correction is more complicated. Furthermore, in the case of a mixed oxide cathodes the compound with the most positive decomposition potential (E^o) will be reduced first, and then the potential will rapidly shift toward that required to reduce the oxide with the next most positive E^o. In this way chronopotentiometry can be utilized to gain an understanding of the electrochemical steps during the electro-deoxidation of a system, and the potentials at which they occur.

The Korea Atomic Energy Research Institute (KAERI) is one of the leading research groups for using the CP technique to investigate the reduction of metal oxide cathodes to metallic powder in molten salt (usually LiCl–Li_2O). However, the concept of the electrochemical reduction process used by KAERI is not necessarily the same as the FFC-Cambridge process. The KAERI approach combined the ionization of oxygen with lithiothermic reduction. The standard decomposition potentials of Li_2O and LiCl are −2.47 and −3.46 V at 923 K respectively, allowing an operating window in which metallic Li could be deposited from Li_2O oxide without producing the undesirable chlorine gas on the anode. Therefore, the metal oxide at the cathode could be reduced, even partially, by the deposited metallic Li. The assemblage

dx.doi.org/10.1021/cr200305x | Chem. Rev. 2013, 113, 2863–2886

used in the electrolysis, consists of a porous MgO basket membrane as a container for the metal oxide powder, and this is connected to the negative terminal through metallic current collectors (Ni or Fe alloys). Pt was used as the anode and as the pseudo reference electrode in most of the investigations, but SnO_2 was also tested.

Uranium oxide has received the greatest attention of the KAERI group's research.[100,116] The reduction of U_3O_8 to UO_2 was found to occur spontaneously in the molten salt.[116a] However, the reduction potential of UO_2 to metallic uranium is very close to the deposition potential of lithium from Li_2O, making the ionization of oxygen from the cathode without Li deposition impractical. Based on the experimental findings in which the concentration of Li_2O in the molten electrolyte decreased during the course of electrolysis according to Faraday's law, Hur et al[116a] suggested the reduction to start by the generation of Li metal from the decomposition of Li_2O, and then the chemical reaction between Li and uranium oxide generating Li^+ and O^{2-} ions. The O^{2-} ions diffuse through the porous magnesia membrane toward the bulk electrolyte and then discharge at the platinum anode evolving oxygen gas.[116a]

However, the direct ionization of the oxygen from uranium oxide cannot be excluded. In reality, the chronopotentiogram in Hur's study (Figure 10) showed a small peak by the end of

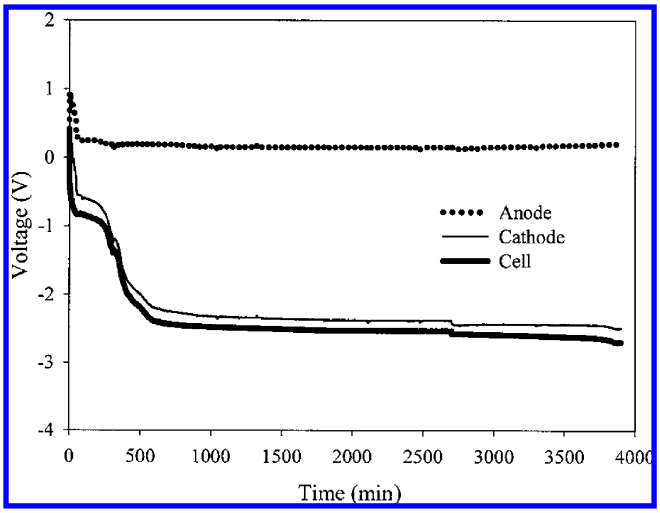

Figure 10. Chronopotentiogram recorded during the reduction of U_3O_8 in Li_2O–LiCl molten salt at constant current of 0.3 A for 45 h and then 0.6 A until the end of the run.[116a] Reprinted with permission from ref 116a. Copyright 2003 Springer.

electrolysis when the applied current was relatively small.[116a] This peak, although small, indicates a change in the redox couple, likely because of the switch from the direct ionization of oxygen to the deposition of lithium. Further evidence that direct ionization might take place is obtained by using a cathode assemblage consisting of a stainless steel mesh container field with uranium oxide powder. Although metallic lithium is now more likely to be deposited outside the mesh because of the conductive nature of stainless steel, about 10% of the uranium oxide was reduced to uranium metal.[117] The observed decrease in the Li_2O content in the melt might be attributed to the formation of lithium–uranium-oxygen intermediate compounds on the cathode, as also observed in a later investigation.[116h]

Further confirmation of the reduction mechanism was obtained by comparing the potential profile recorded upon applying different current densities. At a current density below 106.1 mA/cm^2, the potential increased gradually in the early stages of electrolysis until it reached a plateau of −2.465 V.[116g] Indeed, this potential behavior corresponds to the reduction of U_3O_8 to oxides of a lower oxidation state for uranium, such as U_4O_9, UO_2, or a U–O solid solution, through the direct ionization mechanism since lithium metal cannot be deposited at such low potentials.[116g] Furthermore, XRD analysis for the partially reduced sample[118] detected lithium uranates ($Li_xU_yO_z$), with the intensity of its peaks decreasing with increased charge supplied.[116g] The uranates phases disappeared in the sample with 80% supplied charge.[116g] From the aforementioned results, the reduction mechanism can be concluded to start by the direct ionization of oxygen to form a lower oxidation state of uranium and lithium uranates, which are then reduced to metallic uranium by a combination of direct reduction and electro-metallothermic reduction mechanisms.

The usefulness of the CP technique is manifested in its ability to scale up the electro-deoxidation process. Reduction of a 20-kg batch of uranium oxide with 99% conversion to metallic uranium after 120 h was reported using an adapted chronopotentiometry method.[116b] The applied current was changed stepwise from 40 to 80 A to control the rate of the electrochemical reaction.[116b] After 70 h of operation, the concentration of the Li_2O was found to be lower than 0.5%, which leads to a rapid increase in the anode potential, and a high corrosion of the Pt anode.[116b] Experimentally, Pt was found to oxidized to Pt^{2+} at 2.6 V (vs Li–Pb reference electrode) in the absence of O^{2-} ions, while it forms a protective coating of Li_2PtO_3 at higher Li_2O contents in the melt.[119] Therefore, lithium oxide was added twice to the melt to achieve stable operating conditions for a high reduction conversion.[116b] Moreover, a FeU_6 alloy was simultaneously synthesized during the reduction of a 10 kg batch of U_3O_8 by using a Fe-based cathode.[116f] By forming this alloy, it was possible to melt and consolidate the generated uranium below the temperatures where the oxidation of uranium by Li_2O occurred.[116f]

Similar to the reduction of U_3O_8, the integrated cathode assembly with its porous magnesia membrane was used to reduce Ta_2O_5, in molten LiCl–Li_2O at 923 K, under constant current.[120] The chronopotentiogram obtained for pure Ta_2O_5 (Figure 11) showed a sharp increase in both anode and cathode

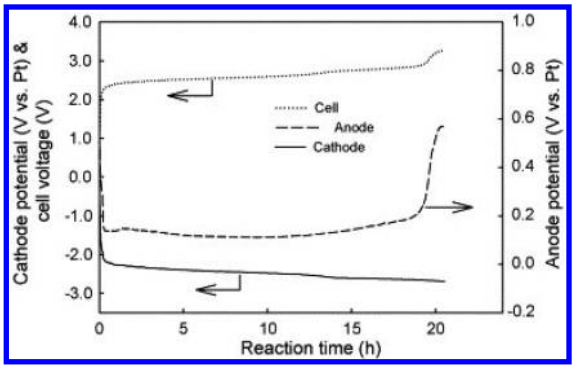

Figure 11. Chronopotentiogram of the electroreduction of Ta_2O_5 in the LiCl–3 wt.% Li_2O at constant current of 1.5 A.[120a] Reprinted with permission from ref 120a. Copyright 2007 Elsevier.

dx.doi.org/10.1021/cr200305x | *Chem. Rev.* 2013, 113, 2863–2886

potential in the first stage, followed by a pseudosteady state in which the cell voltage is around 2.5 V but increases slightly with time.[120] The anode potential was found to increase during the course of electrolysis due to the oxidation on the Pt wire, claimed by the authors to take place by the combined effects of oxygen gas and Li intercalation, forming a protective layer of Li_2PtO_3.[120a] Once the Li_2O was depleted from the electrolyte, a significant increase in the anode potential was observed due to the dissolution of Pt, and the experimental run was terminated.[120a] This trivial increase in the anodic potential, followed by the sharp shift at the end of electrolysis, was not observed when the starting material was lithium tantalate $LiTaO_3$.[120a]

The cathodic potential profiles also showed the same behavior, that is, a slight increase with the reaction time during the pseudosteady state of pure Ta_2O_5 reduction, and an almost constant potential when $LiTaO_3$ was the starting material.[120a] Thus, the slight increase in the potential of Ta_2O_5 cathode might be attributed to the interaction between Li_2O and tantalum oxide leading to the formation of lithium tantalate. Although the decomposition potential of $LiTaO_3$ is about 400 mV more positive than lithium metal deposition,[120] the authors claimed that the reaction proceeded through lithiothermic reduction, with lithium being generated from Li_2O. They used the linear decrease in the Li_2O concentration as proof for a Faradic deposition of Li on the cathode.[99,120a]

However, the chronopotentiogram recorded for Nb_2O_5 (Figure 12) showed a transition stage in which the potential

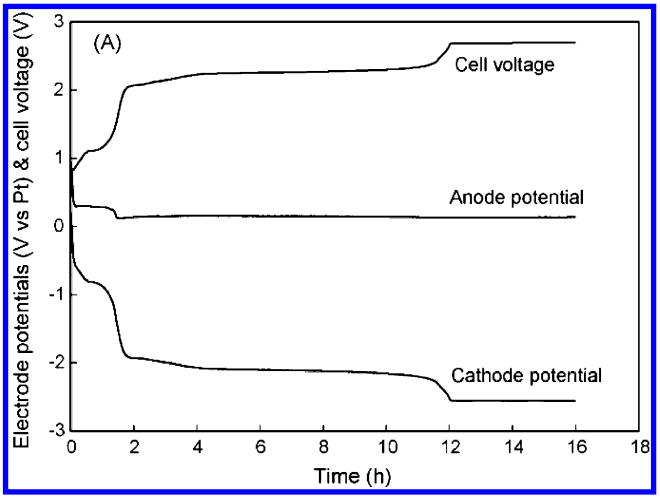

Figure 12. Chronopotentiogram recorded during the reduction of Nb_2O_5 in LiCl-3 wt. % Li_2O at 0.8 A constant current.[121] Reprinted with permission from ref 121. Copyright 2008 Elsevier.

increased gradually before the pseudosteady state potential.[121] The reduction at this stage is without doubt through the direct ionization mechanism, as lithium cannot be deposited at such low potentials. In addition, two distinguished steady potential stages were observed, with the first of them having a potential lower than the decomposition potential of Li_2O.[121] The authors claimed that the deposition of Li could have happened at a potential lower than the theoretical potential in the first stage, due to the EC nature of the process, and the potential shift between the two steady states because of the deposition of Li metal in the inside of the cathode when "the rate of Li generation exceeds the rate of Li consumption by a reaction with the niobium oxides".[121] However, the value of the cell voltage obtained during the Ta_2O_5 reduction process, which also has the same EC nature, was higher than that recorded during Nb_2O_5 reduction, suggesting one of them, at least, is not due to Li_2O decomposition. In fact, these pseudosteady state potentials are more likely to be due to the direct reduction of lithium tantalate and niobate to metallic Ta and Nb, respectively. When the amount of the oxides on the cathode becomes much smaller than that of the metallic phases, that is, not enough supply of ions to maintain the constant current, the cathode potential shifts to that of the more negative redox couple, which explain the two stages of steady potential in the Nb_2O_5 case. The absence of this peak for the case of Ta_2O_5 may be explained by the difference in the experimental conditions. About 7 g of Nb_2O_5 was used per run, while the reduction of Ta_2O_5 was conducted using 30 g of the powder, which mean more Li ions are consumed to form $LiTaO_3$ than $LiNbO_3$, and more oxygen is thus produced on the anode to keep the electrical neutrality of the electrolyte. The diffusion of the oxygen ions generated by the cathodic reaction, and also the byproduct lithium ions, are much slower in the thicker Ta_2O_5 layer and the thicker magnesia membrane, than in Nb_2O_5, leading to Li_2O depletion in the electrolyte and oxygen ions depletion in the vicinity of the anode. This depletion introduced a suitable condition for Pt dissolution, and then the cell was terminated during the electroreduction of Ta_2O_5 before Li deposition occurred.

The diffusion of the generated oxygen ions, and also the lithium ions, from the cathodic reaction to the electrolyte bulk was found to be slow in general and also depended on the oxide (or oxide−metal layer), the applied current, and the size of the membrane. This slow mass transfer explains the continuous decrease in the Li_2O concentration in the melt, as the rate of consumption of the Li_2O to form the lithium−metal−oxygen intermediate is much higher than the rate of recovering both Li^+ and O^{2-} from the bulk electrolyte. Some of the Li_2O is likely to be trapped inside the cathode assemblage lowering the oxide concentration in the bulk electrolyte. Therefore, it was not a surprise result to find Li_2O in the distilled water used for the rinsing of the sample, recovered after SiO_2 reduction in molten Li_2O−LiCl.[122]

The decomposition potential of CaO is higher than that of Li_2O, allowing larger windows between the reduction of the metal oxide on the cathode, and the deposition of the alkaline ions from the electrolyte. Therefore, applying the CP on a CaO−$CaCl_2$ melt should give a clearer idea on the reduction mechanism than in Li_2O−LiCl, particularly if using a consumable graphite anode eliminates the oxidation process on the anode. The chronopotentiogram (Figure 13) recorded for pure cobalt monoxide and pure chromium oxide cathodes, in molten CaO−$CaCl_2$, with a 10 mm-diameter graphite rod being used as an anode, showed some interesting key features.[123] First, the anodic potential was constant and had almost the same value for CoO or Cr_2O_3, indicating the same reactions were occurring with the same rate on the anode.[123] Second, the cathodic potential of Cr_2O_3 was about 1 V higher than that for CoO, revealing different electrochemical reactions involved, that is, it cannot be referred to as CaO decomposition.[123] Third, the cathodic potential shifted sharply to a second electrochemical step giving almost the same cell voltage for both oxides (around 2.8 V), but after different transition times.[123] This voltage value is close to the standard decomposition potential of CaO (2.65 V) at the same temperature, if the *iR* drop is taken into consideration.

dx.doi.org/10.1021/cr200305x | *Chem. Rev.* 2013, 113, 2863−2886

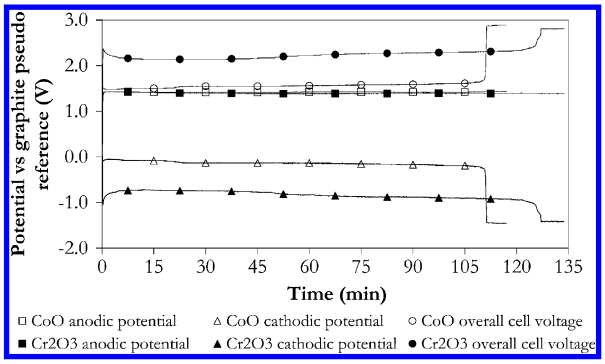

Figure 13. Potential−time curve recoded during the electro-deoxidation of CoO and Cr_2O_3 at 0.5 A constant current.[123] Reprinted with permission from ref 123. Copyright 2010 The Electrochemical Society].

Moreover, when the oxide pellets were wrapped by Ag wire, the cell terminated directly after starting the second electrochemical step, due to the formation of Ag−Ca alloy which has a melting point lower than the operating temperature. Fourthly, the cathodic potential of CoO in the first steady state is almost constant, while that of Cr_2O_3 is slightly increased. The XRD analysis showed $CaCr_2O_4$ phases in the partially reduced chromium oxide, while cobalt oxide did not form any intermediate with calcium oxide.[123] Therefore, the slightly increase in the potential during Cr_2O_3 reduction corresponds to the formation of $CaCr_2O_4$. Finally, the potential difference between the second and the first steady state potential was about 1.5 V in the case of the CoO cathode, and 0.8 V in the case of the Cr_2O_3 cathode.[123] This value is close to the standard decomposition potential of CoO and $CaCr_2O_4$ (which is the expected phase) as measured versus calcium metal deposition. In conclusion, the CP technique proved that the reduction of CoO and Cr_2O_3 takes place by the direct electro-deoxidation mechanism and does not involve any chemical reaction steps.

Considering the reduction of mixed oxide solid solutions to form alloys or intermetallic, CP is a very useful technique to give very interesting mechanistic information about the electrochemical steps during electro-deoxidation. Hyslop et al.,[123] studied the decomposition of $CoCr_2O_4$−CoO solid solution under constant current CP. The potential−time curve showed two steady-state electrochemical steps before the deposition of calcium.[123] The first plateau was confirmed by XRD analysis for the partially reduced sample, to represent the formation of metallic cobalt either from the reduction of CoO (eq 60), or through the simultaneous reduction and substitution of Co^{2+} by Ca^{2+} (reaction 61).[123] The second steady state represents the reduction of $CaCr_2O_4$ to metallic chromium (eq 62).[123] When the chromium ions in the cathode are depleted by complete conversion to metallic Cr, the deposition of metallic calcium starts (eq 63) and the cathodic potential shift to a more negative value.[123]

$$CoO + 2e^- = Co + O^{2-} \quad (60)$$

$$CoCr_2O_4 + Ca^{2+} + 2e^- = CaCr_2O_4 + Co \quad (61)$$

$$CaCr_2O_4 + 6e^- = 2Cr + Ca^{2+} + 4O^{2-} \quad (62)$$

$$Ca^{2+} + 2e^- = Ca + O^{2-} \quad (63)$$

6. SUMMARY AND FUTURE DIRECTION

The electro-deoxidation of solid oxides provides a direct, simple, green, and sustainable alternative to conventional extractive metallurgical methods for the production of metals and alloys. The electro-deoxidation process has been subjected to large number of investigations from many laboratories across the globe during the past decade. The process has been applied to a wide range of single and mixed metal oxides, and many different voltammetry techniques have been used to investigate the chemical mechanisms in detail. These techniques include constant voltage, constant potential, cyclic voltammetry, and constant current.

The electro-deoxidation of mixed oxides used to synthesize alloys and intermetallics in one single step has formed a significant proportion of the research conducted so far in the field of the FFC-Cambridge process. Most of the produced alloys were investigated under constant voltage conditions. The production of alloys allowed further application of the FFC-Cambridge process to produce more sophisticated systems and functional materials.

The work carried out under a controlled cathodic potential indicated that the reduction reactions take place at the oxide−metal−electrolyte three phase interline (3PI), and therefore a theory about the reduction mechanism has been introduced. The electro-deoxidation of any oxide pellet starts by rapid reduction of the surface film according to what is known as the "thin layer three phase interline model". The reduction slows down as it propagates in the depth direction, and the reduction is described through "the penetrating three-phase interline (P3PIs) model". Interrupting the electro-deoxidation at different times confirmed that the reduction takes place in steps according to the oxidation states of the oxide under consideration. Furthermore, intermediate phases resulting from the interaction between the molten electrolyte and the oxide pellets were always observed during the reduction. These intermediate phases play an important role in the kinetic and the energy consumption of the process.

Cyclic voltammetry was used mainly to study the reduction mechanism and kinetics of the electro-deoxidation process. The oxide was used as a working electrode in three distinct forms: (1) an oxide layer formed by the thermal oxidation of metal in air, (2) a small pellet of the oxide powder, and (3) a microscopic hole made in a metal electrode and filled manually with the oxide (metal cavity electrode). Applications of cyclic voltammetry in the context of the electro-deoxidation process include (1) understanding the cathodic reactions by correlating the peak potentials with the thermodynamic calculated potentials, (2) investigating the anodic processes, (3) determining some thermodynamic parameters of the process and subsequently optimizing the production operation conditions, (4) exploring the surface processes like adsorption and oxide layer reduction, (5) studying the complex side processes and detecting the high temperature intermediate phases by comparing the cyclic voltammograms of oxides with the electrochemical windows of a nonredox electrode in the same electrolyte, and (6) to determine the kinetic of the reactions that take place prior to the formation of the metal phase.

The electro-deoxidation of solid oxides under constant current chronopotentiometry was limited to the metals and alloys that have low elemental oxygen solubility, as the dissociation of the salt is kinetically more favorable than

dx.doi.org/10.1021/cr200305x | Chem. Rev. 2013, 113, 2863−2886

ionizing the oxygen from the metal phase. Therefore, metallothermic reduction was combined with the electro-deoxidation process to obtain oxygen content to the part per million level when U_3O_8, Ta_2O_5, and Nb_2O_5 were electro-deoxidized under constant current. Constant current chronopotentiometry also gives very interesting mechanistic information about the electrochemical steps during electro-deoxidation, by studying the electrochemical steps before the decomposition of the electrolyte.

The outlook of the electro-deoxidation process continues to be promising because it offers the prospect of producing a wide range of well-known alloys or developing new systems that were not possible to be achieved through conventional powder metallurgical techniques. In addition, the ability of the process to produce nonstoichiometric compounds under certain conditions opens the door for the application of the electro-deoxidation process in the preparation of functional materials. The process might also revolutionize solid-state electrochemistry if sufficient control is applied to produce pure nonstoichiometric compounds. It is the time now to advance the electro-deoxidation process even further by focusing on the preparation and characterization of such high-tech application materials.

AUTHOR INFORMATION

Corresponding Author

*E-mail: amr.abdelkader@manchester.ac.uk.

Notes

The authors declare no competing financial interest.

Biographies

Amr M. Abdelkader received his MSc in Engineering at Cairo University in 2007 and his Ph.D. in 2011 from the University of Cambridge under the supervision of Prof. Derek J. Fray. Amr has 7 years of experience in sustainable production of metal powders from their raw materials. In context with the FFC-Cambridge process, he published 9 articles. Amr is currently a research fellow at the Faculty of Engineering and Physical Sciences, University of Manchester, where his research focuses on the electrochemical properties of graphene and other 2D materials.

Kamal Tripuraneni Kilby obtained his M.Eng in Chemical Engineering at Imperial College, London, in 2003, an honorary diploma from the Heinlein Trust in 2006, and, his Ph.D. in 2008 with Prof. Derek J. Fray at the University of Cambridge. His doctoral thesis is entitled "The Anodic Synthesis of Oxygen via the FFC-Cambridge Process". Kamal is currently working in industry at Procter and Gamble.

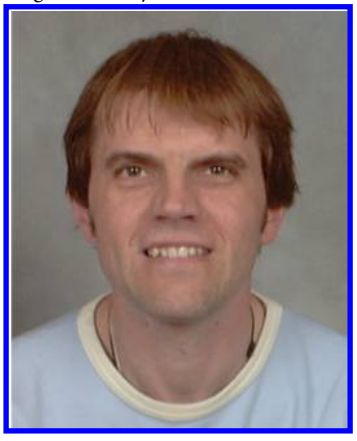

Antony Cox received his BSc with Honours in Chemistry and Biology from the Sheffield City Polytechnic, and obtained his Ph.D. in Corrosion Science from UMIST. He is a senior research associate in prof. Derek Fray's group at the University of Cambridge. Antony has more than 20 years in the field of electrochemistry, and he is one of the pioneer researchers in the field of the FFC-Cambridge process. His research interests focus on high temperature electrochemical engineering applied to extractive metallurgy and recycling with a view to energy economy, low cost, and clean environment.

Derek Fray is Director of Research and Emeritus Professor of Materials Chemistry. He has published over 400 articles on materials processing and one book and is cited as the inventor on over 150 granted patents. Twelve projects are now under active industrial

development both in the U.K. and Europe, Australia, and the United States. He has been awarded the following honours: Matthey Prize, AIME Extractive Metallurgy Technology Award, Sir George Beilby Medal, Kroll Medal, Fellow of the Royal Academy of Engineering, John Phillips Medal, Honorary Professor at the University of Science and Technology, Beijing, Visiting Professor, University of Leeds, Minerals, Metals & Materials Society's 2000 Extraction and Processing Distinguished Lecture Award, Billiton Medal, 2001 Light Metals Reactive Metals Award and a Gold Medal by the Institute of Industrial Science, University of Tokyo, in 2003, Gold Medal by the Institute of Materials and the Armourers and Brasier's Award by the Royal Society. He was also elected a Fellow of the Royal Society of Chemistry. In 2004, he was again awarded the Light Metals Reactive Metals Award and, in 2008, he was elected a Fellow of the Royal Society. In 2009, he was awarded the Federation of European Materials Societies Innovation Award and Prize and in 2012, the Max Bredig Award by the US Electrochemical Society. In 2011, an international conference in his honour was held in Cancun, attended by 450 delegates from 80 countries and conference proceedings extended to 7 volumes and 5000 pages). He is a founder director of Ion Science Ltd., Environmental Monitoring and Control Ltd., Metalysis Ltd., Camfridge Ltd, Inotec, Ltd., and Chinuka Ltd. All these companies are exploiting technology developed by Derek Fray.

REFERENCES

(1) Dircks, H. *Contribution Towards a History of Electro-metallurgy*; E.&F.N. Spon: London, U.K., 1863.

(2) Habashi, F. *Handbook of Extractive Metallurgy*; Wiley-VCH: Weinheim, Germany, 1997.

(3) Ward, R. G.; Hoar, T. P. *J. Inst. Met.* **1961**, *90*, 6.

(4) (a) Okabe, T. H.; Deura, T. N.; Oishi, T.; Ono, K.; Sadoway, D. R. *J. Alloys Compd.* **1996**, *237*, 150. (b) Okabe, T. H.; Nakamura, M.; Oishi, T.; Ono, K. *Metall. Trans. B* **1993**, *24*, 449. (c) Hirota, K.; Okabe, T. H.; Saito, F.; Waseda, Y.; Jacob, K. T. *J. Alloys Compd.* **1999**, *282*, 101.

(5) (a) Chen, G. Z.; Fray, D. J.; Farthing, T. W. *Metall. Mater. Trans. B* **2001**, *32*, 1041. (b) Fray, D. J.; Chen, G. Z.; Farthing, T. W. Int. Patent WO9964638, 1999.

(6) (a) Chen, G. Z.; Fray, D. J.; Farthing, T. W. *Nature* **2000**, *407*, 361. (b) Tripathy, P. K.; Gauthier, M.; Fray, D. J. *Metall. Mater. Trans. B* **2007**, *38*, 893.

(7) (a) Wang, D.; Jin, X.; Chen, G. Z. *Annu. Rep. Prog. Chem., Sect. C: Phys. Chem.* **2008**, *104*, 45. (b) Fray, D. J.; Chen, G. Z. *Mater. Sci. Technol.* **2004**, *20*, 295. (c) Fray, D. J. *Trans. Inst. Min. Metall., Sect. C* **2006**, *115*, 3. (d) Chen, G. Z. *Trans. Electrochem. Soc.* **2008**, 205.

(8) (a) Suzuki, R. O.; Ono, K. Presented at the TMS Annual Meeting San Diego, USA, 2003. (b) Suzuki, R. O.; Teranuma, K.; Ono, K. *Metall. Mater. Trans. B* **2003**, *34*, 287. (c) Ono, K.; Suzuki, R. *JOM* **2002**, *54*, 59. (d) Suzuki, R. O. *J. Phys. Chem. Solids* **2005**, *66*, 461.

(9) (a) Fray, D. J. *Can. Metall. Q.* **2002**, *41*, 433. (b) Mohandas, K. S.; Fray, D. J. *Trans. Indian Inst. Met.* **2004**, *57*, 579.

(10) Roine, A. In *HSC Chemistry*; Outotec Oyj Research: Espoo, Finland, 2008.

(11) Littlewood, R. *J. Electrochem. Soc.* **1962**, *109*, 525.

(12) (a) Picard, G.; Seon, F.; Tremillon, B. *J. Electroanal. Chem.* **1979**, *102*, 65. (b) Combes, R.; Levelut, M. N.; Tremillon, B. *J. Electroanal. Chem.* **1978**, *91*, 125.

(13) Dring, K.; Dashwood, R.; Inman, D. *J. Electrochem. Soc.* **2005**, *152*, D184.

(14) (a) Jackson, B.; Jackson, M.; Dye, D.; Inman, D.; Dashwood, R. *J. Electrochem. Soc.* **2008**, *155*, E171. (b) Bhagat, R.; Jackson, M.; Inman, D.; Dashwood, R. *J. Electrochem. Soc.* **2008**, *155*, E63. (c) Bhagat, R.; Jackson, M.; Inman, D.; Dashwood, R. *J. Electrochem. Soc.* **2009**, *156*, E1.

(15) Okabe, T. H.; Suzuki, R. O.; Oishi, T.; Ono, K. *Mater. Trans., JIM* **1991**, *32*, 485.

(16) Motion of the electrolyte with respect to the electrode arises as a result of density gradients building up at the electrode surface because of differences in density between reactants and products.

(17) (a) Fray, D. J. *JOM* **2001**, *53*, 26. (b) Chen, G. Z.; Fray, D. J. In *Light Metals*; Anjier, J. L., Ed.; Minerals, Metals & Materials Society: Warrendale, PA, 2001. (c) Fray, D. J.; Chen, G. Z.; Icmr, I. I. In *Proceedings of the Fourth International Conference on Materials Engineering for Resources*, Vol *1*; Akita University: Akita-ken, Japan, 2001.

(18) Chen, G. Z.; Fray, D. J. *Light Met.* **2001**, 1147.

(19) Yan, X. Y.; Fray, D. J. *Metall. Mater. Trans. B* **2002**, *33*, 685.

(20) Schwandt, C.; Fray, D. J. *Z. Naturforsch. A* **2007**, *62*, 655.

(21) Yan, X. Y.; Fray, D. J. *J. Mater. Res.* **2003**, *18*, 346.

(22) Chen, G. Z.; Fray, D. J. *Proceedings of the 6th International Symposium on Molten Salt Chemistry and Technology*, Shanghai, 2001; Trans Tech Publications, Ltd.: Durnten-Zurich, Switzerland, 2001; p 79.

(23) Chen, G. Z.; Gordo, E.; Fray, D. J. *Metall. Mater. Trans. B* **2004**, *35*, 223.

(24) (a) Xiao, W.; Jin, X. B.; Deng, Y.; Wang, D. H.; Hu, X. H.; Chen, G. Z. *ChemPhysChem* **2006**, *7*, 1750. (b) Deng, Y.; Wang, D. H.; Xiao, W.; Jin, X. B.; Hu, X. H.; Chen, G. Z. *J. Phys. Chem. B* **2005**, *109*, 14043. (c) Xiao, W.; Jin, X. B.; Deng, Y.; Wang, D. H.; Chen, G. Z. *Chem.—Eur. J.* **2007**, *13*, 604. (d) Jin, X. B.; Gao, P.; Wang, D. H.; Hu, X. H.; Chen, G. Z. *Angew. Chem., Int. Ed.* **2004**, *43*, 733.

(25) Chen, G. Z.; Fray, D. J. *Miner. Process. Extr. Metall.* **2006**, *115*, 49.

(26) (a) Yan, X. Y.; Fray, D. J. *Adv. Funct. Mater.* **2005**, *15*, 1757. (b) Yan, X. Y.; Fray, D. J. In *Light Metals 2002*; Schneider, W. A., Ed.; Minerals, Metals & Materials Society: Warrendale, PA, 2002.

(27) Xu, Q.; Deng, L. Q.; Wu, Y.; Ma, T. *J. Alloys Compd.* **2005**, *396*, 288.

(28) Barnett, R., PhD Thesis, University of Cambridge, Cambridge, U.K., 2008.

(29) Song, Q.-s.; Xu, Q.; Kang, X.; Du, J.-h.; Xi, Z.-p. *J. Alloys Compd.* **2010**, *490*, 241.

(30) Wu, T.; Jin; Xiao, W.; Hu; Wang; Chen, G. Z. *Chem. Mater.* **2006**, *19*, 153.

(31) Gordo, E.; Chen, G. Z.; Fray, D. J. *Electrochim. Acta* **2004**, *49*, 2195.

(32) (a) Wang, S. L.; Li, Y. J. *J. Electroanal. Chem.* **2004**, *571*, 37. (b) Ratchev, I.; Bliznyukov, S.; Olivares, R.; Watts, R. O. *Cost-Affordable Titanium —Symposium Dedicated to Professor Harvey Flower*; Minerals, Metals & Materials Society: Warrendale, PA, 2004; p 209 (c) Chen, G. Z.; Fray, D. J. In *Light Metals 2004*; Tabereaux, A. T., Ed.; Minerals, Metals & Materials Soc: Warrendale, 2004. (d) Dring, K.; Jackson, M.; Dashwood, R.; Flower, H.; Inman, D. In *Cost-Affordable Titanium—Symposium Dedicated to Professor Harvey Flower*; Froes, F. H., Imam, M. A., Fray, D., Eds.; Minerals, Metals & Materials Society: Warrendale, PA, 2004. (e) Ma, M.; Jiang, K.; Qiu, G. H.; Wang, D. H.; Hu, X. H.; Jin, X. B.; George, C. Z. *J. Rare Earths* **2005**, *23*, 46. (f) Jiang, K.; Hu, X. H.; Ma, M.; Wang, D. H.; Qiu, G. H.; Jin, X. B.; Chen, G. Z. *Angew. Chem., Int. Ed.* **2006**, *45*, 428. (g) Nie, X. M.; Dong, L. Y.; Bai, C. G.; Chen, D. F.; Qiu, G. B. *Trans. Nonferrous Met. Soc. China* **2006**, *16*, S723. (h) Ma, M.; Wang, D. H.; Wang, W. G.; Hu, X. H.; Jin, X. B.; Chen, G. Z. *J. Alloys Compd.* **2006**, *420*, 37. (i) Du, J. H.; Xi, Z. P.; Li, Q. Y.; Li, Z. X.; Tang, Y. *Rare Met. Mater. Eng.* **2006**, *35*, 1045. (j) Mishra, P. K.; Mohanty, J.; Rath, P. C.; Nayak, B. B.; Paramguru, R. K. *Trans. Indian Inst. Met.* **2006**, *59*, 463. (k) Du, J. H.; Xi, Z. P.; Li, Q. Y.; Li, Z. X.; Tang, Y. *Rare Met. Mater. Eng.* **2007**, *36*, 96. (l) Centeno-Sanchez, R. L.; Fray, D. J.; Chen, G. Z. *J. Mater. Sci.* **2007**, *42*, 7494. (m) Qiu, G. H.; Jiang, K.; Ma, M.; Wang, D. H.; Jin, X. B.; Chen, G. Z. *Z. Naturforsch. A* **2007**, *62*, 292. (n) Lu, M. F.; Lu, S. G.; Kan, S. R.; Li, G. X. *Rare Metals* **2007**, *26*, 547. (o) Park, J. I.; Jung, J. Y. *J. Korean Inst. Met. Mater.* **2007**, *45*, 567. (p) Zhai, X. J.; Zhang, Z.; Li, J. D.; Zhang, M. J. In *TMS 2008 Annual Meeting Supplemental Proceedings, Vol 1: Materials Processing and Properties*; Minerals, Metals & Materials Society: Warrendale, PA, 2008. (q) Yang, X. B.; Lahiri, A.; Jha, A. In *Energy Technology Perspectives: Conservation,*

Carbon Dioxide Reduction and Production from Alternative Sources; Neelameggham, N. R., Reddy, R. G., Belt, C. K., Vidal, E. E., Eds.; Minerals, Metals & Materials Soc: Warrendale, PA, 2009. (r) Schwandt, C.; Fray, D. J. *Electrochim. Acta* **2005**, *51*, 66. (s) Alexander, D. T. L.; Schwandt, C.; Fray, D. J. *Acta. Mater.* **2006**, *54*, 2933. (t) Schwandt, C.; Alexander, D. T. L.; Fray, D. J. *Electrochim. Acta* **2009**, *54*, 3819. (u) Li, W.; Jin, X. B.; Huang, F. L.; Chen, G. Z. *Angew. Chem., Int. Ed.* **2010**, *49*, 3203. (v) Deng, L. Q.; Xu, Q.; Ma, T.; Li, B.; Zhai, Y. C. *Acta Metall. Sin.* **2005**, *41*, 551. (w) Mohanty, J.; Rath, P. C.; Subbaiah, T.; Mishra, K. G.; Paramguru, R. K. *Trans. Indian Inst. Met.* **2009**, *62*, 249.

(33) Li, Q. Y.; Du, J. H.; Xi, Z. P.; Li, Z. X.; Yang, S. H. *Rare Met. Mater. Eng.* **2009**, *38*, 1575.

(34) Bhagat, R.; Dye, D.; Raghunathan, S. L.; Talling, R. J.; Inman, D.; Jackson, B. K.; Rao, K. K.; Dashwood, R. J. *Acta. Mater.* **2010**, *58*, 5057.

(35) Wu, T.; Xiao, W.; Jin, X.; Liu, C.; Wang, D.; Chen, G. Z. *Phys. Chem. Chem. Phys.* **2008**, *10*, 1809.

(36) Abdelkader, A. M.; Daher, A.; Abdelkareem, R. A.; El-Kashif, E. *Metall. Mater. Trans. B* **2007**, *38*, 35.

(37) Jacob, K. T.; Gupta, S. *Bull. Mater. Sci.* **2009**, *32*, 611.

(38) Garvie, R. C.; Nicholso, Ps. *J. Am. Ceram. Soc.* **1972**, *55*, 152.

(39) Li, Q. Y.; Du, J. H.; Xi, Z. P. *Trans. Nonferrous Met. Soc. China* **2007**, *17*, S560.

(40) Mohandas, K. S.; Fray, D. J. *Metall. Mater. Trans. B* **2009**, *40*, 685.

(41) Peng, J.; Jiang, K.; Xiao, W.; Wang, D.; Jin, X.; Chen, G. Z. *Chem. Mater.* **2008**, *20*, 7274.

(42) Li, Q. Y.; Du, J. H.; Xi, Z. P. *Rare Metal Mat. Eng.* **2007**, *36*, 390.

(43) Mohandas, K. S.; Fray, D. J. *J. Appl. Electrochem.* **2011**, *41*, 321.

(44) Erdogan, M.; Karakaya, I. *Metall. Mater. Trans. B* **2010**, *41*, 798.

(45) Yan, X. Y. *Metall. Mater. Trans. B* **2008**, *39*, 348.

(46) Cox, A.; Fray, D. J. *Molten Salts XIII*; Pennington: El Dorado Hills, CA, 2002; p 745.

(47) (a) Xie, H. W.; Zhang, H.; Zhai, Y. C.; Wang, J. X.; Li, C. D. *J. Mater. Sci. Technol.* **2009**, *25*, 459. (b) Yin, H. Y.; Gao, L. L.; Zhu, H.; Gan, F. X.; Wang, D. H.; Tms In *TMS 2010 139th Annual Meeting*; Minerals, Metals & Materials Society: Warrendale, PA, 2010.

(48) Yan, X. Y.; Fray, D. J. *J. Appl. Electrochem.* **2009**, *39*, 1349.

(49) (a) Glowacki, B. A.; Fray, D. J.; Yan, X. Y.; Chen, G. *Phys. C* **2003**, *387*, 242. (b) Glowacki, B. A.; Yan, X. Y.; Fray, D.; Chen, G.; Majoros, M.; Shi, Y. *Phys. C* **2002**, *372*, 1315.

(50) Meng, F. K.; Lu, H. M. *Adv. Eng. Mater.* **2009**, *11*, 198.

(51) Abdelkader, A. M.; Fray, D. J. *Electrochim. Acta* **2010**, *55*, 2924.

(52) Xu, Q.; Schwandt, C.; Fray, D. *Adv. Mater. Res.* **2011**, *160*−*162*, 1131.

(53) Yan, X. Y.; Fray, D. J. *J. Alloys Compd.* **2009**, *486*, 154.

(54) (a) Dashwood, R.; Jackson, M.; Dring, K.; Rao, K.; Bhagat, R.; Inman, D. In *Innovations in Titanium Technology*; Wiley: Hoboken, NJ, 2007 (b) Dring, K.; Bhagat, R.; Jackson, M.; Dashwood, R.; Inman, D. *J. Alloys Compd.* **2006**, *419*, 103.

(55) (a) Ma, M.; Wang, D. H.; Hu, X. H.; Jin, X. B.; Chen, G. Z. *Chem.—Eur. J.* **2006**, *12*, 5075. (b) Tan, S.; Oers, T.; Aydinol, M. K.; Ozturk, T.; Karakaya, I. *J. Alloys Compd.* **2009**, *475*, 368. (c) Li, G. M.; Jin, X. B.; Wang, D. H.; Chen, G. Z. *J. Alloys Compd.* **2009**, *482*, 320. (d) Panigrahi, M.; Paramguru, R. K.; Gupta, R. C.; Shibata, E.; Nakamura, T. *High Temp. Mater. Process.* **2010**, *29*, 495.

(56) Guo, X.; Guo, Z.; Wang, Z. *J. Univ. Sci. Technol. B.* **2008**, *30*, 620.

(57) Liao, X.; Zhai, Y.; Xie, H.; Zhang, Y. *Chin. J. Mater. Res.* **2009**, *23*, 133.

(58) Centeno, S. R. L.; Chen, G. Z.; Fray, D. J. *Chiang Mai J. Sci.* **2005**, *32*, 367.

(59) Meng, F. K.; Lu, H. M. In *EPD Congress 2009, Proceedings*; Howard, S. M., Ed.; Minerals, Metals & Materials Society: Warrendale, PA, 2009.

(60) Zou, X. L.; Lu, X. G.; Li, C. H.; Zhou, Z. F. *Electrochim. Acta* **2010**, *55*, 5173.

(61) Osaki, S.; Sakai, H.; Suzuki, R. O. *J. Electrochem. Soc.* **2010**, *157*, E117.

(62) Liu, M.; Lu, S.; Kan, S. *Chin. J. Rare Met.* **2008**, *32*, 526.

(63) Peng, J. J.; Chen, H. L.; Jin, X. B.; Wang, T.; Wang, D. H.; Chen, G. Z. *Chem. Mater.* **2009**, *21*, 5187.

(64) Wang, D. H.; Qiu, G. H.; Jin, X. B.; Hu, X. H.; Chen, G. Z. *Angew. Chem., Int. Ed.* **2006**, *45*, 2384.

(65) (a) Qiu, G. H.; Wang, D. H.; Jin, X. B.; Chen, G. Z. *Electrochim. Acta* **2006**, *51*, 5785. (b) Qiu, G. H.; Wang, D. H.; Jin, X. B.; Chen, G. Z. *Acta Metall. Sin.* **2008**, *44*, 859.

(66) Xie, H. W.; Wang, J. X.; Zhai, Y. C.; Li, C. D.; Liao, X. J. *J. Northeastern Univ.* **2009**, *30*, 180.

(67) Xie, H.; Zhai, Y.; Liao, X.; Wang, J. *J. Rare Earths* **2005**, *23*, 93.

(68) Zhao, B. J.; Wang, L.; Dai, L.; Cui, G. G.; Zhou, H. Z.; Kumar, R. V. *J. Alloys Compd.* **2009**, *468*, 379.

(69) (a) Zhao, B. J.; Lu, X. G.; Wang, L.; Cui, G. H. *Rare Met. Mater. Eng.* **2010**, *39*, 1089. (b) Gao, Y.; Zhao, H.; Zhou, Z.; Mao, L.; Peng, M. *Adv. Mat. Res.* **2011**, *189*−*193*, 575.

(70) Zhang, Q. J.; Tian, Y.; Wang, L.; Dai, L.; Li, Y. H.; Qu, M. L.; Cui, C. X. *J. Func. Mater* **2010**, *41*, 1257.

(71) Kang, X.; Xu, Q.; Ma, S.; Zhao, L. *Proceeding for the 2008 Joint Symposium on Molten Salt*, October 2008, Japan; Deki, S., Ota, K., Eds.; MS8 Secretariat: Kobe, Japan, 2008; p 313.

(72) Zhu, Y.; Wang, D. H.; Ma, M.; Hu, X. H.; Jin, X. B.; Chen, G. Z. *Chem. Commun.* **2007**, 2515.

(73) Abdelkader, A. M.; Hyslop, D. J. S.; Cox, A.; Fray, D. J. *J. Mater. Chem.* **2010**, *20*, 6039.

(74) Muir Wood, A. J.; Copcutt, R. C.; Chen, G. Z.; Fray, D. J. *Adv. Eng. Mater.* **2003**, *5*, 650.

(75) Zhu, Y.; Ma, M.; Wang, D. H.; Jiang, K.; Hu, X. H.; Jin, X. B.; Chen, G. Z. *Chin. Sci. Bull.* **2006**, *51*, 2535.

(76) Jackson, B. K.; Inman, D.; Jackson, M.; Dye, D.; Dashwood, R. J. *J. Electrochem. Soc.* **2010**, *157*, E36.

(77) Jackson, B. K.; Dye, D.; Inman, D.; Bhagat, R.; Talling, R. J.; Raghunathan, S. L.; Jackson, M.; Dashwood, R. J. *J. Electrochem. Soc.* **2010**, *157*, E57.

(78) Tan, S.; Aydinol, K.; Ozturk, T.; Karakaya, I. *J. Alloys Compd.* **2010**, *504*, 134.

(79) Peng, J. J.; Jiang, K.; Xiao, W.; Wang, D. H.; Jin, X. B.; Chen, G. Z. *Chem. Mater.* **2008**, *20*, 7274.

(80) Peng, J. J.; Zhu, Y.; Wang, D. H.; Jin, X. B.; Chen, G. Z. *J. Mater. Chem.* **2009**, *19*, 2803.

(81) (a) Pistorius, P. C.; Fray, D. J. *J. South. Afr. Inst. Min. Metall.* **2006**, *106*, 31. (b) Suzuki, R. O.; Fukui, S. *Mater. Trans.* **2004**, *45*, 1665.

(82) Kilby, K. C. T.; Centeno, L.; Doughty, G.; Mucklejohn, S.; Fray, D. J. *Space Resources Roundtable VIII*, Oct 31− Nov 2, 2006, Golden, CO; Colorado School of Mines: Golden, CO, 2006; p 64.

(83) Kilby, K. PhD Thesis, University of Cambridge, Cambridge, U.K., 2008.

(84) (a) Burheim, O.; Haarberg, G. M. *Miner. Process. Extr. Metall.* **2010**, *119*, 77. (b) Kvalheim, E.; Haarberg, G. M.; Martinez, A. M.; Jahren, H. M. *Trans. Electrochem. Soc.* **2009**, *16*, 367.

(85) (a) Pistorius, P. C.; Fray, D. J. *J. South. Afr. Inst. Min. Metall.* **2006**, *106*, 31. (b) Groult, H.; Kaplan, B.; Lantelme, F.; Komaba, S.; Kumagai, N.; Yashiro, H.; Nakajima, T.; Simon, B.; Barhoun, A. *Solid State Ionics* **2006**, *177*, 869.

(86) Jiao, S. Q.; Kumar, K. N. P.; Kilby, K. T.; Fray, D. J. *Mater. Res. Bull.* **2009**, *44*, 1738.

(87) Barnett, R.; Kilby, K. T.; Fray, D. J. *Metall. Mater. Trans. B* **2009**, *40*, 150.

(88) Jiao, S. Q.; Fray, D. J. *Metall. Mater. Trans. B* **2010**, *41*, 74.

(89) Jiao, S. Q.; Kilby, K. T.; Zhang, L. J.; Fray, D. J. *Nanotechnology* **2009**, 20.

(90) Jiao, S.; Zhang, L.; Zhu, H.; Fray, D. J. *Electrochim. Acta* **2010**, *55*, 7016.

(91) (a) Cox, A.; Fray, D. J. *Ironmaking Steelmaking* **2008**, *35*, 561. (b) Cox, A.; Fray, D. *J. Appl. Electrochem.* **2008**, *38*, 1401. (c) Cox, A.;

Fray, D. J. *TMS Annual Meeting*; Minerals, Metals & Materials Society: Warrendale, PA, 2009; p 77.
(92) Bard, A. J.; Faulkner, L. R. *Electrochemical Methods: Fundamentals and Applications*, 2nd ed.; John Wiley: New York, 2001.
(93) Amatore, C. A.; Jutand, A.; Pfluger, F. *J. Electroanal. Chem.* **1987**, *218*, 361.
(94) Heinze, J. *Angew. Chem., Int. Ed. Engl.* **1984**, *23*, 831.
(95) Izutsu, K. D. *Electrochemistry in Nonaqueous Solutions*, 2nd ed.; Wiley-VCH: Weinheim, Germany, 2009.
(96) Chen, G. Z.; Fray, D. J. *J. Electrochem. Soc.* **2002**, *149*, E455.
(97) Dring, K.; Dashwood, R.; Inman, D. *J. Electrochem. Soc.* **2005**, *152*, E104.
(98) Qiu, G. H.; Ma, M.; Wang, D. H.; Jin, X. B.; Hu, X. H.; Chen, G. Z. *J. Electrochem. Soc.* **2005**, *152*, E328.
(99) Qiu, G. H.; Feng, X. H.; Liu, M. M.; Tan, W. F.; Liu, F. *Electrochim. Acta* **2008**, *53*, 4074.
(100) Park, B. H.; Park, S. B.; Jeong, S. M.; Seo, C. S.; Park, S. W. *J. Radioanal. Nucl. Chem.* **2006**, *270*, 575.
(101) Hur, J. M.; Jeong, S. M.; Lee, H. *Electrochem. Commun.* **2010**, *12*, 706.
(102) Nohira, T.; Yasuda, K.; Ito, Y. *Nat. Mater.* **2003**, *2*, 397.
(103) (a) Yasuda, K.; Nohira, T.; Takahashi, K.; Hagiwara, R.; Ogata, Y. H. *J. Electrochem. Soc.* **2005**, *152*, D232. (b) Yasuda, K.; Nohira, T.; Hagiwara, R.; Ogata, Y. H. *J. Electrochem. Soc.* **2007**, *154*, E95.
(104) Yasuda, K.; Nohira, T.; Ogata, Y. H.; Ito, Y. *J. Electrochem. Soc.* **2005**, *152*, D208.
(105) Yasuda, K.; Nohira, T.; Hagiwara, R.; Ogata, Y. H. *Electrochim. Acta* **2007**, *53*, 106.
(106) Xiao, W.; Jin, X. B.; Deng, Y.; Wang, D. H.; Chen, G. Z. *J. Electroanal. Chem.* **2010**, *639*, 130.
(107) (a) Yasuda, K.; Nohira, T.; Ogata, Y. H.; Ito, Y. *Electrochim. Acta* **2005**, *51*, 561. (b) Mohamedi, M.; Borresen, B.; Haarberg, G. M.; Tunold, R. *J. Electrochem. Soc.* **1999**, *146*, 1472.
(108) Peng, J. J.; Li, G. M.; Chen, H. L.; Wang, D. H.; Jin, X. B.; Chen, G. Z. *J. Electrochem. Soc.* **2010**, *157*, F1.
(109) Mohandas, K. S.; Fray, D. J. *Metall. Mater. Trans. B* **2009**, *40*, 685.
(110) Ackermann, R. J.; Garg, S. P.; Rauh, E. G. *J. Am. Ceram. Soc.* **1977**, *60*, 341.
(111) (a) Dring, K.; Dashwood, R.; Inman, D. *J. Electrochem. Soc.* **2005**, *152*, E104. (b) Dring, K. Thesis, Imperial College, London, 2005.
(112) Sand, H. J. S. *Philos. Mag.* **1901**, *1*, 45.
(113) (a) Dahmen, E. A. M. F. *Electroanalysis: Theory and Applications in Aqueous and Non-aqueous Media and in Automated Chemical Control*; Elsevier: Amsterdam, 1986. (b) Murray, R. W. Chronoamperometry, Chronocoulometry and Chronopotentiometry. In *Physical Methods of Chemistry*; Weissberger, A., Rossiter, B. W., Ed.; Wiley-Interscience: New York, 1971. (c) Rieger, P. H. *Electrochemistry*, 2nd ed.; Chapman & Hall: New York, 1994.
(114) Murray, R. W.; Reilley, C. N. *J. Electroanal. Chem.* **1962**, *3*, 64.
(115) Reinmuth, W. H. *Anal. Chem.* **1961**, *33*, 485.
(116) (a) Hur, J. M.; Seo, C. S.; Hong, S. S.; Kang, D. S.; Park, S. W. *React. Kinet. Catal. Lett.* **2003**, *80*, 217. (b) Jeong, S. M.; Park, S. B.; Hong, S. S.; Seo, C. S.; Park, S. W. *J. Radioanal. Nucl. Chem.* **2006**, *268*, 349. (c) Seo, C. S.; Park, S. B.; Park, B. H.; Jung, K. J.; Park, S. W.; Kim, S. H. *J. Nucl. Sci. Technol.* **2006**, *43*, 587. (d) Park, S. B.; Park, B. H.; Jeong, S. M.; Hur, J. M.; Seo, C. S.; Choi, S. H.; Park, S. W. *J. Radioanal. Nucl. Chem.* **2006**, *268*, 489. (e) Jeong, S. M.; Hur, J. M.; Hong, S. S.; Kang, D. S.; Choung, M. S.; Seo, C. S.; Yoon, J. S.; Park, S. W. *Nucl. Technol.* **2008**, *162*, 184. (f) Hur, J. M.; Choi, I. K. U.; Cho, S. H.; Jeong, S. M.; Seo, C. S. *J. Alloys Compd.* **2008**, *452*, 23. (g) Park, B. H.; Lee, I. W.; Seo, C. S. *Chem. Eng. Sci.* **2008**, *63*, 3485. (h) Park, B. H.; Lee, I. W.; Seo, C. S. *J. Chem. Eng. Jpn.* **2008**, *41*, 294.
(117) Hur, J. M.; Seo, C. S.; Hong, S. S.; Kang, D. S.; Park, S. W. *Proceedings for the Seventh Information Exchange Meeting on Actinide and Fission Product Partitioning and Transmutation*, Jeju, Republic of Korea, 2002; Nuclear Energy Agency: Issy-les-Moulineaux, France, 2002; p 355.
(118) Determined by the different percentage supply of the of the theoretically required charges for complete reduction of the loaded U3O8.
(119) Jeong, S. M.; Shin, H. S.; Cho, S. H.; Hur, J. M.; Lee, H. S. *Electrochim. Acta* **2009**, *54*, 6335.
(120) (a) Jeong, S. M.; Jung, J. Y.; Seo, C. S.; Park, S. W. *J. Alloys Compd.* **2007**, *440*, 210. (b) Seo, C. S.; Jeong, S. M.; Park, S. B.; Jung, J. Y.; Park, S. W.; Kim, S. H. *J. Chem. Eng. Jpn.* **2006**, *39*, 77.
(121) Jeong, S. M.; Yoo, H. Y.; Hur, J. M.; Seo, C. S. *J. Alloys Compd.* **2008**, *452*, 27.
(122) Lee, S. C.; Hur, J. M.; Seo, C. S. *J. Ind. Eng. Chem.* **2008**, *14*, 651.
(123) Hyslop, D. J. S.; Abdelkader, A. M.; Cox, A.; Fray, D. J. *J. Electrochem. Soc.* **2010**, *157*, E111.